Integrating thermal, geological and hydrogeologic methods to study fractured carbonate rock hydrogeology

Erin Mundy

Department of Civil Engineering and Applied Mechanics

McGill University

Montreal, Quebec, Canada

December 2015

A thesis submitted to McGill University in partial fulfillment of the requirements of the degree of Master of Science in Civil Engineering

©Erin Mundy 2015

Acknowledgements

Firstly, I would like to thank my supervisor, Prof. Tom Gleeson, for offering me the opportunity to work on such an interesting project. Your support, guidance, and encouragement helped me greatly throughout the many twists and turns of this "Murphy's Law in hydrogeology" thesis. You have helped me grow and succeed in ways I never thought possible, and I am forever grateful. Thank you.

Secondly, I would like to thank all of the people who helped me during these two projects. Many thanks to Chuck Courcy and Tony Drapelick, as well as the Episcopal Diocese in Burlington, VT, who let us have access to the beautiful field-site at Lone Rock Point and were so helpful during our many visits. Thanks to drilling companies, Cushing and Sons, and Parratt-Wolff, who provided quality work, despite the crazy karst system we encountered. Also, a big thank you to Kelian Dascher-Cousineau and Christie Rowe for the structural data and input on the Champlain Thrust manuscript, and to Diana Allen for the help with aquifer-pumping tests. Thanks to Jean Dubreuil who let us have access to the quarry in St. Dominique, QC, even though our request may have seemed strange (who takes pictures of water on rocks?!). Thanks to Hillary Topps for being an amazing field assistant at the quarry - thank you for keeping me sane during the 24-hour experiment!

I would also like to thank my family and Brett Montgomery for being a source of laughter and encouragement throughout this experience. Even though you guys did not understand the work I was doing, you all helped just by simply being the crazy characters you are. Thank you!

Lastly, but certainly not least, I would like to thank my best friends, Mark Ranjram and Mikhail Smilovic, for their never-ending support and encouragement throughout these past two years. Thank you guys for believing in me, even when I did not believe in myself. Through the laughter, tears, and near-death experiences, you guys have helped shape me into the person I am today and made my graduate school experience unforgettable. Words cannot express how thankful I am to have met you guys and have you in my life. Many thanks from "Nerves" Mundy.

Contribution of Authors

This thesis is written as two manuscripts submitted or to be submitted for publication in peer-reviewed journals, in accordance to the guidelines established by McGill University's Graduate and Postdoctoral Studies Office.

The papers from Chapter 3 and Chapter 4 in this thesis are as follow:

Chapter 3: Mundy, E., Gleeson, T., Roberts, M., and J. McKenzie. “Thermal imagery of groundwater seeps: possibilities and limitations”.

Chapter 4: Mundy, E., Dascher-Cousineau, K., Gleeson, T., Rowe, C. and D. Allen. “Complexity of hydrogeologic regime around an ancient low-angle thrust fault revealed by multi-disciplinary field study”.

The author of this thesis is the primary author in all papers included in this thesis. Professor Tom Gleeson was the supervisor of the author’s Master of Science program and is included as co-author in both manuscripts. Professor Gleeson contributed in developing the initial research proposal, guided in the conceptualization of the project, data collection and analysis, and edited the thesis. Prof. Jeffrey McKenzie is a co-supervisor of thermal imagery research on groundwater seeps and is included as co-author of the second manuscript. Mark Roberts collected a portion of the data in the first manuscript (“winter observations”) and included as co-author. M.Sc. student Kelian Dascher-Cousineau collected and co-authored the structural geology section of the second paper and is included as co-author of the second manuscript. Professor Christie Rowe helped refine and edit this portion of the manuscript and is included as co-author. Professor Diana Allen helped with the interpretation of the aquifer pumping test data and edited this manuscript and is included as co-author.

Table of Contents

List of Tables

List of Figures

Abstract

Proper management of carbonate rock aquifers requires an understanding of the aquifers hydraulic properties and flow dynamics. Faulted carbonate rock aquifers have complex permeability patterns, as faults can act as hydraulic conduits, barriers or combined conduit-barrier systems. Integrated, multi-disciplinary methods are needed in order to gain a more comprehensive understanding of fractured carbonate rock hydrogeology. The objective of this thesis is to use thermal, geological and hydrogeologic methods to better understand fractured rock hydrogeology of carbonate rocks. This was completed using two study areas: 1) an unused quarry in St. Dominique, Quebec, Canada, and 2) an outcrop of the Champlain Thrust fault at Lone Rock Point, Burlington, Vermont, USA. Thermal imagery of groundwater seeps at the quarry was collected over a 22-month period to determine the efficacy of using thermal imagery to quantify groundwater discharge. Thermal imagery is effective at locating and qualitatively characterizing the flux of groundwater seeps. However, the application of thermal imagery is limited by diverse factors including technical issues of image acquisition, diurnal changes in radiation and temperature, and rock face heterogeneity. Groundwater discharge rates could not be directly quantified from thermal imagery in either winter or summer because of these limitations. At the outcrop of the Champlain Thrust fault, structural geology observations were integrated with surficial and subsurface hydrogeological observations. Here, the fault core thickness thickens on the meter-scale, splays out into multiple strands and is offset by a minor normal fault. Groundwater seeps are prevalent in the heavily fractured footwall but limited in the fault core and hanging wall, suggesting at the cliff face the water table is generally near the fault core and groundwater flow in the hanging wall is limited. At the well field, the Champlain Thrust fault is offset significantly by a high-angle structure, the water table is near the surface and aquifer pumping tests reveal a complex hydrogeologic system, with karst and steep fractures as strong hydraulic conduits in the hanging wall and fault core. The most salient features of the fault zone hydrogeology in the surface and subsurface data are different but can be integrated into a preliminary conceptual model. Together the surface and subsurface methods underscore and emphasize the complexity and heterogeneity of the hydrogeology of this low angle sedimentary fault.

Résumé

Une bonne gestion des aquifères des roches carbonatées nécessite une compréhension des aquifères propriétés hydrauliques et dynamique de l'écoulement. Faillées aquifères des roches carbonatées ont des motifs de perméabilité complexes, comme des défauts peuvent agir comme des conducteurs hydrauliques, des barrières ou des systèmes combinés conduit-barrière. Méthodes intégrées, multi-disciplinaires sont nécessaires afin d'obtenir une compréhension plus complète de la fracture hydrogéologie carbonate de roche. L'objectif de cette thèse est d'utiliser des méthodes thermiques, géologiques et hydrogéologiques afin de mieux comprendre fracturé hydrogéologie de roche des roches carbonatées. Cela a été fait en utilisant deux zones d'étude: 1) une carrière utilisé à Saint-Dominique, Québec, Canada, et 2) un affleurement de la faute de poussée Champlain à Lone Rock Point, Burlington, Vermont, USA. L'imagerie thermique des eaux souterraines suinte à la carrière ont été recueillies sur une période de 22 mois. L'imagerie thermique est efficace à localiser et caractériser qualitativement le flux des suintements d'eau souterraine. Cependant, l'application de l'imagerie thermique est limitée par divers facteurs, y compris des questions techniques d'acquisition d'image, les changements diurnes de rayonnement et de la température, et le visage de roche hétérogénéité. Taux de décharge des eaux souterraines ne pouvaient pas être directement quantifiés de l'imagerie thermique dans soit l'hiver ou l'été en raison de ces limitations. À l'affleurement de la faille Champlain poussée, observations de géologie structurale ont été intégrés avec les observations hydrogéologiques surface et de subsurface. Ici, l'épaisseur de l'âme de défaut épaissit sur le compteur échelle, évase dehors dans plusieurs brins et est compensée par une faille normale mineur. Suintements d'eau souterraine sont répandues dans l'éponte inférieure fortement fracturée mais limité dans le noyau de la faute et tenture murale, suggérant à la falaise face à la table de l'eau est généralement à proximité du cœur de la faute et des eaux souterraines écoulement dans l'éponte supérieure est limitée. Dans le champ ainsi, la faute Champlain poussée est compensé de manière significative par une structure-grand angle, la nappe phréatique est près de la surface et essais de nappe pompage révéler un système hydrogéologique complexe, avec aussi fortes conduites hydrauliques karstiques et de fractures abruptes dans l'éponte supérieure et reprocher à coeur. Les traits les plus saillants de l'hydrogéologie de la zone de faille dans les données de surface et de subsurface sont différents mais peuvent être intégrées dans un modèle conceptuel préliminaire. Ensemble, les méthodes de surface et de subsurface soulignent et mettent l'accent sur la complexité et de l'hétérogénéité de l'hydrogéologie de ce défaut faible angle sédimentaire.

Chapter 1. Introduction

Fractured rock aquifers are utilized as a groundwater source for several regions around the world. To properly manage the resources supplied by these aquifers requires an understanding of their hydraulic properties and flow dynamics. Depending on the nature of the rock and degree of fracturing, these properties can vary significantly, often displaying considerable heterogeneity between the higher permeablility fractures and lower permeability rock matrix (Lemiuex et al., 2006). Fractured rocks that have displacement, known as faults, also show considerable heterogeneity and variability in permeability. Faults are known to have a dominant impact of numerous hydrologic and geologic processes, such as regional groundwater flow, carbon sequestration, and hydrothermal fluid circulation. Constraining fault zone properties is especially important for many engineering issues, such as nuclear waste repositories or mining contamination, because faults have the capacity to act as barriers to fluid flow, conduits, or a combination of both. Therefore, determining the properties of fault zones is imperative for several environmental concerns. Although several studies have contributed to understanding fluid flow dynamics and transport in fractured rock (see recent reviews by Faulkner et. al., 2010; Bense et al., 2013,) there is still much to be understood (Lemieux et al., 2006). Moreover, despite the abundance of fault zone studies, fault zone permeability is still poorly constrained (Bense et al., 2013).

While there is a large and growing body of work on fractured and fault zone hydrogeology in siliciclastic and crystalline rocks, very few detailed groundwater studies in carbonate rocks are reported (Celico et al., 2006; Lemieux et al., 2006; Bastesen and Braathen, 2010). Approximately 25% of the world's population is supplied drinking water by carbonate rock aquifers (Goldscheider and Drew, 2007). Therefore, research is needed to protect and understand this vital resource. Faults in carbonate rocks exhibit a broad range of hydrogeologic behaviors; from effective conduits, channeling groundwater along fault and fracture planes, to significant barriers due to the formation of fine-grained cataclastic fault rocks (Bense et al., 2013). Springs or groundwater seeps are common along faulted carbonate rocks. Groundwater seeps influence the hydroecology and water budgets of lakes, rivers and oceans, but are underestimated by current methods that aim to quantify seepage flux. Therefore, improved measurement methods are needed.

In order to gain a more comprehensive understanding of fractured rock hydrogeology, integrated, multi-disciplinary approaches are necessary. New integrative methods are especially crucial. For example, temperature has long been recognized as a useful hydrologic tracer, due to the identifiable thermal signature of groundwater. However, recent studies have used thermal infrared imagery to characterize groundwater seepage, providing a non-invasive, easily transferrable method for groundwater studies. Another innovative method to characterize fractured rock hydrogeology requires the combined research by structural geologists and hydrogeologists. Structural geologists and hydrogeologists use different methods to characterize faults and fractured rock. Structural geologists primarily examine outcrops and rock samples to identify fault zone attributes, while hydrogeologists predominately focus on subsurface evidence from wells and springs. By combining these two valuable types of research, a more comprehensive understanding of fractured rock hydrogeology can be obtained. This thesis aims to use thermal imagery and structural and hydrogeological observations to create a better understanding of fractured carbonate rock hydrogeology.

1.1. Study objectives and organization of thesis

The objective of this thesis is to use thermal, geological and hydrogeologic methods to better understand fractured rock hydrogeology of carbonate rocks. This was completed using two study areas: 1) an unused quarry in St. Dominique, Quebec, Canada, and 2) an outcrop of the Champlain Thrust fault at Lone Rock Point, Burlington, Vermont, U.S.A. The unused quarry in St. Dominique was chosen as one of the study areas based on the highly fractured nature of the exposed rock, which resulted in the formation of a significant number of groundwater seeps. Thermal imagery of these seeps was collected over a 22-month period to evaluate the efficacy of thermal imagery for quantifying groundwater discharge in fractured rock terrain. Specific objectives at this field site were:

1) Capture thermal images of groundwater seeps during the winter (3 visits) and summer (3 visits), and record physical observations of seeps during each visit, such as visible flow rate and notable geologic features
2) Capture 24-hours of time lapse thermal imagery of high and low flow seeps
3) Create and capture thermal imagery of an artificial seep experiment at the quarry

4) Analyze the thermal images using a vertical temperature gradient, which represents the change in groundwater temperature with vertical distance down the cliff face, to determine the relationship between groundwater discharge and temperature gradient from thermal imagery

5) Evaluate the possibilities and limitations of thermal imagery for quantifying groundwater discharge

At the Lone Rock Point field site, the Champlain Thrust fault is exposed along the shore of Lake Champlain. This exposure provides the opportunity for both structural and hydrogeologic field observations. Specific objectives at this field site were:

6) Determine prominent structural features of the Champlain Thrust fault

7) Make observations of the groundwater seeps present on the outcrop

8) Plan, drill, and complete wells near the outcrop and determine aquifer parameters from aquifer pumping tests in these wells

9) Relate structural geology to the surficial and subsurface hydrogeologic features to establish a preliminary understanding of the Champlain Thrust fault hydrogeology

Chapter 2 provides an overview of the relevant literature for groundwater flow around fault zones, with particular focus on fractured carbonate rock, as well as methods for studying fractured rock hydrogeology. The first five objectives of the thesis are covered in Chapter 3, which focuses the possibilities and limitations of thermal imagery to quantify groundwater seepage. Chapter 4 addresses objectives 6 - 9 and focuses on integrating structural and hydrogeological data to provide a preliminary hydrogeologic understanding of a carbonate thrust fault. Chapter 5 summarizes key conclusions and suggestions for future research.

Chapter 2. Literature Review

Characterizing and understanding fluid flow in fractured rock aquifers is essential, as faults are known to have a dominant impact on numerous hydrologic and geologic processes. Faults affect groundwater flow patterns (Mayer et al., 2007; Bense et al., 2008; Burbey, 2008), hydrothermal fluid circulation (Berkowitz, 2002; Faulkner et al., 2010) and CO_2 sequestration (Shipton et al., 2004; Agosta et al., 2008). Additionally, faults act as repositories petroleum resources (Aydin, 2000; Sorkhabi and Tsuji, 2005), and affect the storage of nuclear waste (Bredehoeft, 1997; Douglas et al., 2000). Determining the hydraulic properties of fault zones is very important for understanding the processes governing fluid flow in these areas, which is vital for numerous societal concerns. Therefore, determining the hydraulic properties of fault zones is very important for understanding the controls governing subsurface fluid flow in these areas. Despite its importance, the impact of faults on fluid flow is often poorly understood, as the hydraulic properties of fault zones vary greatly, depending on the lithology of the host rock, geologic setting, state of stress, and temporal evolution of the fault (Smith et al., 1990; Scholz and Anders, 1994; Caine et al., 1996; Lopez and Smith, 1996; Bense et al., 2013).

In this section, we first describe the theoretical background of fault zones, describing the widely recognized conceptual model of a fault, and address the difficulty of characterizing fault zone permeability. Particular focus is placed on carbonate rocks, as both field areas within this thesis were within a carbonate geologic setting. Secondly, we describe the different approaches structural geologists and hydrogeologists use to characterize fault zones. We describe both methods to bring attention to the necessity of integrated research by both structural geologists and hydrogeologists to characterize fault zone hydrogeology. Lastly, we discuss the use of temperature as a hydrologic tracer for groundwater flow paths. More specifically, the use of thermal imagery in recent years to characterize groundwater springs and seeps.

2.1. Theoretical background

Fault zones are often described as composed of distinct components: a fault core, damage zone and a protolith (Figure 1; Chester and Logan, 1986; Caine et al., 1996;

Kolyukhin and Torabi, 2012). The fault core is defined as the central structure of the fault zone where most of the displacement and strain occurs (Caine et al., 1996). Single slip-surfaces, unconsolidated clay-rich gouge zones, cataclastic zones, and brecciated and geochemically altered zones are all distinctive of fault cores (Sibson, 1977; Anderson et al., 1983; Chester and Logan, 1986; Caine et al., 1991). Fault cores display low permeability, due to grain size reduction and/or mineral precipitation, which results in fault cores often acting as a barrier to fluid flow (Caine et al., 1996). The damage zone is a distributed network of fractures and faulting that surrounds the fault core. The damage zone is related to the growth of the fault, producing subsidiary structures such as veins, folds, cleavage, small fractures and faults. These structures cause heterogeneity and anisotropy in the permeability structure of the fault, which often enhances fault zone permeability relative to the fault core and protolith (Bruhn et al., 1994; Caine et al., 1996). For example, the permeability of the damage zone in the Dixie Valley fault is four to six orders of magnitude greater than the fault core, and two to three orders of magnitude greater than the permeability of the protlith (Caine et al., 1996). The protolith, or country rock, surrounds the damage zone and the fault core, and displays properties representative of the unfaulted host rock (Caine et al., 1996).

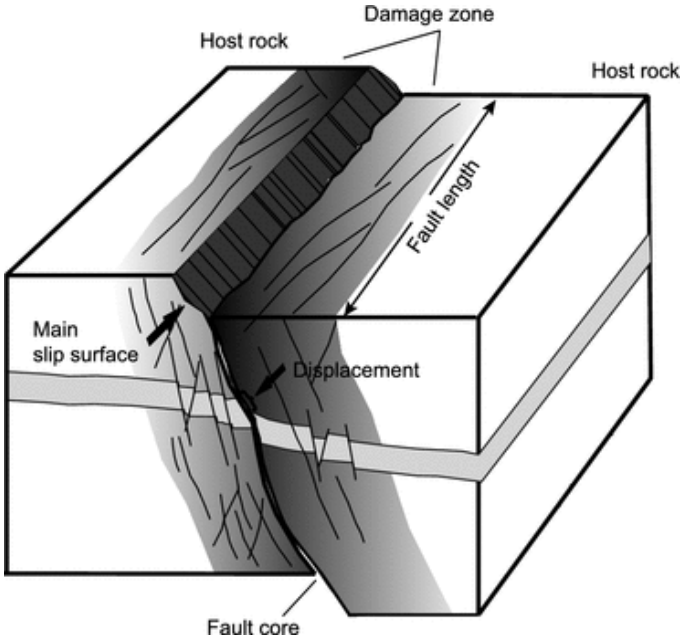

Figure 1. Conceptual model of fault zone (from Kolyukhin and Torabi, 2012).

The permeability structure of a fault zone depends on the relative percentage of the fault core and damage zone structures. Based on this premise, a conceptual scheme for fault related fluid flow in upper-crustal, brittle fault rocks was developed by Caine et al. (1996) (Fig. 2). This conceptual scheme distinguishes four categories of fault zone permeability: localized conduit, distributed conduit, localized barrier or combined conduit-barrier systems. When the damage zone is absent or poorly developed, a fault will act either as a localized conduit, if the fault core is narrow, or a localized barrier, if the fault core is wide. Similarly, when the damage zone is wide relative to the fault core, the fault will act as a distributed conduit. When the fault core and the damage zone are both well developed, the fault will act as a combined conduit-barrier system, with enhanced fault-parallel permeability and reduced fault-perpendicular permeability (Caine et al., 1996).

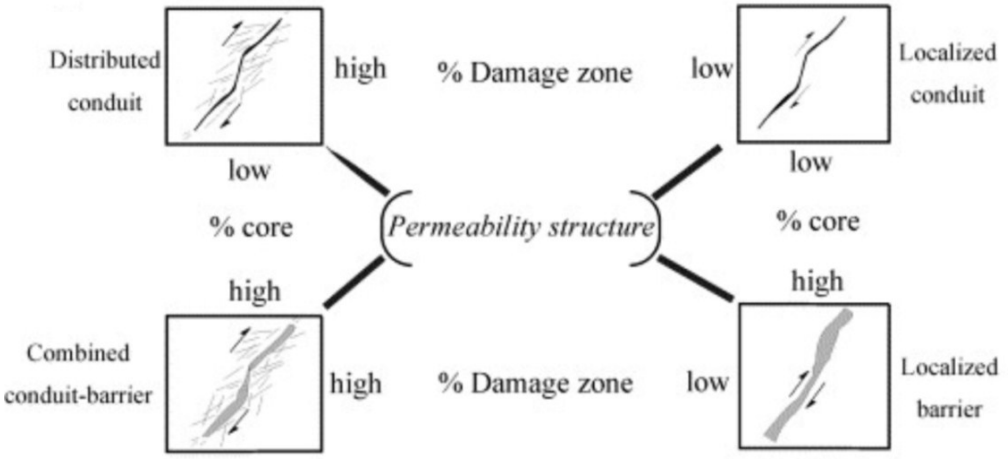

Figure 2. Conceptual scheme for fault-related fluid flow (from Caine et al., 1996).

The conduit-barrier schematics of fault zones depend greatly on the geometry and magnitude of permeability contrasts between the fault core and damage zone (Caine et al., 1996). The fault core has significantly less fracture density, as compared to the damage zone. Therefore, grain-scale permeability of the fault rocks controls the permeability of the fault core, and the distributed fracture network controls the damage zone permeability (Caine et al., 1996).

Characterizing fault components and their permeability is challenging, as fault components are heterogeneous and anisotropic, with varying permeability temporally and spatially (Faulkner et al., 2010). Additionally, it is often difficult to determine the

morphological position (ie. fault core, damage zone or protolith) of which the samples were collected (Evans, 1990). Furthermore, the network connectivity and fracture aperture, which partly control the permeability, are typically unknown away from the test wells (Long and Billaux, 1987; Evans, 1990; Bense et al., 2013). For example, field data was used to create a discrete fracture model of a uranium mine in Fanay-Augeres, France (Long and Billaux, 1987). The results of this study showed the difficulty in predicting which fractures are conductive, as only ~0.1% of the fractures essentially controlled the permeability. Thus, the permeability of fault zones is governed by the permeability of individual fractures and fault rocks in addition to their geometric three-dimensional architecture (Lunn et al., 2008).

2.2. Fault zone hydrogeology of carbonate rocks

Approximately 25% of the world's population is supplied drinking water by carbonate rock aquifers (Goldscheider and Drew, 2007). Weathering and dissolution are common in carbonate rocks, which greatly increases the permeability, resulting in important aquifers. Faults in carbonate rocks exhibit a broad range of hydrogeologic behaviours, with fracturing, cataclasis, and dissolution weathering playing significant roles affecting permeability (Billi et al., 2007; Bense et al., 2013). Faults can act as significant barriers due to secondary cementation (Micarelli et al., 2006), smearing of low permeability material (e.g. clay gouge) into the fault core (Agosta and Kirschner, 2003; Doan and Cornet, 2007), or the formation of fine-grained cataclastic fault rocks (Agosta and Kirschner, 2003; Celico et al., 2006). Pressure gradients observed from borehole data across fault zones can provide evidence as to whether the fault is acting as a barrier to fluid flow. Such was the case for Giurgea et al. (2004), where a water pressure difference greater than 0.5 MPa was observed across the fault plane, indicating that the Aigon fault zone (Greece) acts as a hydraulic barrier. Faults in carbonate rocks can also act as effective conduits, due to brecciation, dilatational jogs, and uncemented fracture networks (Andrews et al., 1982; Billi et al., 2007; Bense et al., 2013). Additionally, combined of conduit-barrier systems have been recorded in carbonate rock faults (Breesch et al., 2009). For example, pumping tests in a carbonate aquifer in Ottawa, Ontario revealed the presence of both permeable fracture networks and barriers along the faults (Allen and Michel, 1999).

While there is a large and growing body of work on fault zone hydrogeology in siliciclastic and crystalline rocks, there is a paucity of detailed groundwater studies in carbonate rocks, especially fractured dolostone (Celico et al., 2006; Lemieux et al., 2006; Bastesen and Braathen, 2010). Moreover, the few that have been documented are heavily focused on strike slip faults or normal faults (Lemeiux et al., 2006; Micarelli et al., 2006; Agosta et al., 2007).

2.3. Approaches to fault zone hydrogeology

Structural geologists and hydrogeologists employ different methods and approaches to characterizing fault zone architecture and permeability. To effectively study fault zone hydrogeology, combined research by structural geologists and hydrogeologists is needed. The different methods taken by each respective discipline are discussed below.

2.3.1. Structural geology approach

Structural geologists mainly focus on surficial studies to identify fault zone attributes. When the fault is well exposed at the surface, structural geologists map the outcrop, measuring fault zone characteristics such as the length, orientation and aperture of the fractures (Bense et al., 2013). For example, Jourde et al. (2002) determined large-scale equivalent permeabilities of strike-slip faults in porous sandstone in the Valley of Fire State Park, Nevada by mapping outcrops. Other useful outcrop observations include the nature of fracture termination, presence of mineralization, staining and surface roughness (Novakowski et al., 2007). As groundwater flows through a fracture, minerals can precipitate, leaving an impermeable infilled fracture. Characterizing fault rock mineralogy and geochemistry can give insight into water-rock interactions, paleoflow orientations and permeability structure of the fault (Mozley and Goodwin, 1995; Breesch et al., 2009). For example, Caine and Minor (2009) used geochemical evidence to interpret deformation and groundwater flow along the San Ysidro fault in New Mexico.

Structural geologists can study subsurface fault zone characteristics from logging core or geophysical techniques, such as seismic, ground penetrating radar (GPR), and electromagnetic surveys, to name a few. Geophysical data can be used to characterize the morphology of fault zones within the subsurface, as seismic waves will reflect differently

at geologic interfaces where a change in density and velocity occurs (Dorn et al., 2012) For example, Grandjean and Gourry (1996) used ground penetrating radar to produce a detailed image of the fractures within a marble quarry in Thassos, Greece, thereby distinguishing the marketable marble areas within the quarry.

Rock core is obtained from diamond-drilled boreholes and can be used to determine subsurface fractures patterns and potential groundwater flow paths (Kulander et al., 1990; West et al., 2005; Novakowski et al., 2007). Rock core displays important geologic contacts and features and allows for the direct observation of fractures, which is very useful for assessing fault zone properties. Discontinuities in lithology are frequently preferential flow paths for groundwater (Novakowski et al., 2007). Additionally, laboratory tests on rock core can measure the small-scale patterns of permeability of fault structures (Amaefule et al., 1993; Baker et al., 2013).

The data collected from these methods are used to create conceptual models and numerical models of fault zones (Caine et al., 1996; Aydin, 2000; Bense et al., 2013). However, direct hydrogeological evidence of hydraulic behavior supporting these models is often lacking (Bense et al., 2013).

2.3.2. Hydrogeology approach

Conversely, hydrogeologists focus mainly on subsurface studies to determine the hydrogeologic behavior of fault zones and do not characterize fault zone architecture or observe fault structure in outcrop. Instead, hydrogeologists collect direct hydrogeologic evidence from wells and springs in order to determine groundwater flow paths along fault zones. Hydrogeologists often face challenges when studying fault zone hydrogeology, as groundwater-monitoring networks are rarely placed over fault zones.

Hydrogeologists use various hydraulic testing methods to determine the hydrogeological properties of fault zones. Several pieces of equipment are essential for hydraulic testing: pressure transducer, water level measure, water pump, and packers. Packers are used to seal off portions of a borehole, which allows for testing of a specific zone. Pressure transducers measure the pressure response in the isolated section as water is injected or withdrawn from the borehole via slug tests or pumping tests. Hydraulic head gradients at the fault zone, as determined by water level measurements, can be used

to infer groundwater flow paths and rate of fluid flow at the fault zone (Bense et al., 2003). The results from these tests are then used to determine the hydrogeologic properties of the fault zone (Novakowski et al., 2007).

In conjunction with hydraulic head observations, groundwater geochemistry, temperature, and age can be used to determine groundwater flow paths along faults. Natural tracers for groundwater, like salinity, can constrain fluid flow paths around faults. For example, saline tracers were applied to fractured thrust fault aquifer in Virginia, USA, revealing that faults in crystalline rock can act as combined conduit-barrier systems (Rugh and Burbey, 2008). Thermal anomalies, due to significant groundwater flow, have been used to delineate groundwater flow paths along faults. In the Lower Rhine Embayment in Germany, thermal anomalies were recorded in aquifers bordering the Rurrand fault. This could only be explained by the fault acting as a conduit, channeling significant groundwater flow along the fault, which then laterally migrates into nearby aquifers (Bense et al., 2008). Groundwater age dating uses the known decay rates of radioactive isotopes to estimate the age of a groundwater sample, which can be used to infer groundwater flow paths along faults (Bethke and Johnson, 2008). Flint et al. (2001) used bomb pulse isotopes (ie. ^{36}Cl) to assess groundwater ages along faults in the Yucca mountain, Nevada, USA. These isotopes were highly elevated in the atmosphere during the early 1960's, due to nuclear testing in the Pacific Ocean. The groundwater age was determined to be less than 40 years old, which suggests the faults act as conduits, with deep, rapid movement along the faults.

Hydrogeologists use analytical and numerical models for interpreting fault zone hydrogeology. Numerical models are designed as discrete fracture network models or continuum models, and can be used to test conceptual models and parameter estimations. Large-scale hydrogeologic models (10-100s km) are typically grid-based continuum models that represent bulk permeability of the fault components or fault zone, whereas discrete fracture network models use detailed geometric and hydraulic data to explicitly represent the orientation, shape, connectivity, and aperture of discrete fractures (Bense et al., 2013).

2.4. Temperature and thermal imagery of groundwater seeps

Temperature is widely recognized as a useful hydrologic tracer, able to detect stream-aquifer interaction, delineate flow through fractures, and identify hydrologic thermal heterogeneity (Anderson, 2005). This is because groundwater has an identifiable thermal signature, being relatively constant throughout the year, as compared to surface water or land surfaces, which vary on diurnal and seasonal cycles (Anderson, 2005; Deitchman and Loehide, 2009). The temperature of groundwater is relatively cool compared to air temperature in the summer, and relatively warmer in the winter. There has been a renewed interest in using thermal imagery as a hydrologic tracer recently, largely because of the development of low cost temperature-sensing equipment (Pandey et al., 2013). As a result, thermal imagery is now utilized in a variety of hydrogeologic environments.

Thermal imagery has been used in recent studies to detect groundwater springs and qualitatively characterize seepage faces (Loehide and Gorelick, 2006; Waldick and Conant, 2006). For example, Deitchman and Loehide (2009) demonstrated that thermal imagery could be used to distinguish between unsaturated and saturated zones on a stream bank seepage face, thereby locating the position of the water table. Pfister et al. (2010) used thermal imagery to identify the location and connectivity of variably saturated areas in a hillslope-riparian-stream system and determined that thermal imagery can be used to distinguish areas with snow cover, snow melt and soil seepage. Thermal imagery has also been used in controlled laboratory experiments to quantify groundwater discharge flux. Pandey et al. (2013) determined that thermal imagery could be used to predict groundwater flow under low flow conditions in a cold room laboratory. However, this relationship has not been verified by field observations. While these studies have made significant progress, it is currently not possible to directly quantifying groundwater discharge in the field using thermal imagery without utilizing thermal mixing models or heat budgets (Pandey et al., 2013).

2.4.1. Seepage faces

Groundwater seepage is common along cliff faces, hill slopes, and stream banks. Seepage faces influence the hydroecology and water budgets of watersheds, lakes, rivers

and oceans, but are rarely included in groundwater modelling (Simpson et al., 2003). Seepage faces are not traditionally used in groundwater modelling because their effects are considered insignificant due to their small percentage of the modelling domain (at the aquifer scale) or when computational inadequacy makes their representation unfeasible (Romanoa et al., 1999). In riparian zones, the influence of seepage faces on hydrologic and ecologic processes is underestimated by current methods of quantifying seepage face groundwater flux; improved measurement methods are required to describe the interaction between groundwater and these important ecological niches (Deitchman and Loehide, 2009).

Chapter 3. Thermal imagery of groundwater seeps: possibilities and limitations

3.1. Introduction

Temperature has long been recognized as a useful hydrologic tracer, able to detect stream-aquifer interaction, identify hydrologic thermal heterogeneity, and delineate flow through fractures (Anderson, 2005). Groundwater has an identifiable thermal signature, due to its relatively constant temperature throughout the year, as compared to surface water or land surfaces, which vary on diurnal and seasonal cycles (Anderson, 2005; Deitchman and Loehide, 2009). Groundwater temperature is relatively cool compared to air temperature in the summer, and relatively warmer in the winter. Recently, there has been a renewed interest in using thermal imagery as a hydrologic tracer, mainly due to the development of low cost temperature-sensing equipment (Anderson, 2005; Loehide and Gorelick, 2006; Waldick and Conant, 2006; Deitchman and Loehide, 2009; Pfister et al., 2010; Pandey et al., 2013; Dugdale et al., 2015). This has expanded the application of thermal imagery to a variety of hydrogeologic environments and has the potential to further develop temperature as a hydrologic tracer (Pandey et al., 2013).

Recent studies have focused on using thermal imagery to detect groundwater springs and qualitatively characterize seepage faces (Loehide and Gorelick, 2006; Waldick and Conant, 2006). For example, Pfister et al. (2010) used ground-based thermal imagery to identify the location and connectivity of variably saturated areas in a hillslope-riparian-stream system. Deitchman and Loehide (2009) demonstrated that thermal imagery could be used to locate the position of the water table of a stream bank seepage face, as well as distinguish between areas of low, moderate and high groundwater discharge at the seepage face boundary. Additionally, Deitchman and Loehide (2009) observed that thermal imagery provided insight to the differences between diffuse and focused groundwater flow, demonstrating that groundwater flow is more discrete and heterogeneous than commonly modelled. In addition to field studies, thermal imagery has also been used in laboratory experiments to quantify groundwater discharge. Pandey et al. (2013) demonstrated that thermal infrared imagery could be used to predict groundwater flow under low flow conditions in a cold room laboratory. However, this relationship has not

been verified with field experiments. Although these studies have made significant progress, directly quantifying groundwater discharge in the field using thermal imagery has not been possible without utilizing thermal mixing models or heat budgets (Pandey et al., 2013).

Groundwater flows out of the subsurface, known as "seepage," when the pressure head is zero at an external boundary in a saturated zone (Boufadel et al., 1999). Seepage faces influence the hydroecology and water budgets of lakes, rivers and oceans and are common along cliff faces, hill slopes, and stream banks. Seepage faces are characteristic of shallow, unconfined groundwater systems, but are seldom included in groundwater modelling (Simpson et al., 2003). This is because at the aquifer scale (>10km^2), seepage faces make up a small percentage of the modeling domain and their influence on the overall water balance is assumed to be negligible (Romanoa et al., 1999). Additionally, at this scale, discretization restrictions may prevent the representation of seepage faces (Romanoa et al., 1999). More recent modelling approaches account for seepage faces by coupling surface water processes directly to groundwater (e.g. Brunner et al., 2009), or specific seepage algorithms (Batelaan and De Smedt, 2005). In riparian zones, the influence of seepage faces on hydrologic and ecologic processes is underestimated by current methods of quantifying seepage face groundwater flux; improved measurement methods are required to describe the interaction between groundwater and these important ecological niches (Deitchman and Loehide, 2009).

Our objective is to determine the possibilities and limitations of thermal imagery in quantifying groundwater discharge from seepage faces. Specifically, the efficacy of thermal imagery for quantifying groundwater discharge in fractured rock is evaluated. The conditions under which thermal imagery are applicable, including geology, sun exposure, and season, are evaluated and discussed. Our analysis is motivated by the hypothesis that groundwater discharging from a seepage face at a high flow rate may not appreciably warm as it travels down a cliff face in the summer (or appreciably cool as it travels in the winter), whereas groundwater with a lower flow rate may experience more warming (or cooling, depending on the season). Therefore the change in groundwater temperature with vertical distance from the seep origin, herein called the vertical temperature gradient, observed from a thermal image may be a function of the discharge rate. A low vertical temperature gradient corresponds to a small change in temperature with vertical distance down the cliff face, whereas a high vertical temperature

gradient refers to significant changes in temperature with vertical distance. To the best of our knowledge, this relationship has not been quantified in literature.

3.2. Field Area and Methods

An unused quarry located in Saint Dominique, Quebec, Canada, was chosen as the field site due to the large number of groundwater seeps at the site and due to the structure of the quarry itself, with four sides that experience varying levels of sunlight and three elevation zones representing distinct depths beneath the surface. A fractured rock site was selected for this analysis because seeps from fractured rock tend to be more distinct than seeps from porous media. Initial analysis of the field site showed no obvious correlation between seepage flow rate and location, and no clustering of seeps at a specific elevation level or side of the quarry, thereby allowing us to consider the effect of sun exposure on the observed thermal gradients. The climate has a high seasonality (mean January temperature: -10.2°C; mean July temperature: 20.6°C), making the quarry an appropriate location to examine the evolution of groundwater seeps in different seasons using thermal imagery. The geology of the quarry consists of Middle Ordovician limestone with thin beds of shale. The rocks were faulted and folded by a single thin-skinned deformation phase of the Paleozoic Taconian orogeny, which involved multiple phases of cross-cutting faults and folds. Taconian structures were subsequently deformed by oblique brittle structures and cross-cut by small and localized volcanic dykes (Séjourné and Malo, 2007).

Thermal and optical images of the groundwater seeps within the quarry were collected during seven field visits that took place between January 2013 and October 2014 to capture the impact of seasons on characterizing groundwater seeps with thermal imagery (Fig. 3). The time of visits was determined based on local weather forecasts in order to encompass a range of weather conditions. For example, in January 2013, the field visits coincided with a period of prolonged below freezing conditions so that the effect of extreme cold on the development of the ice seeps could be analyzed. Similarly, the field visit in February 2013 took place after a rise in temperature to above freezing, whereby the effect of warmer temperatures on ice seep development could be observed. The field visits during the summer of 2014 took place under cloudy, warm conditions (June and September,) as well as sunny and hot conditions (August), in order to distinguish the effect warmer temperatures have on seep development (Table 1).

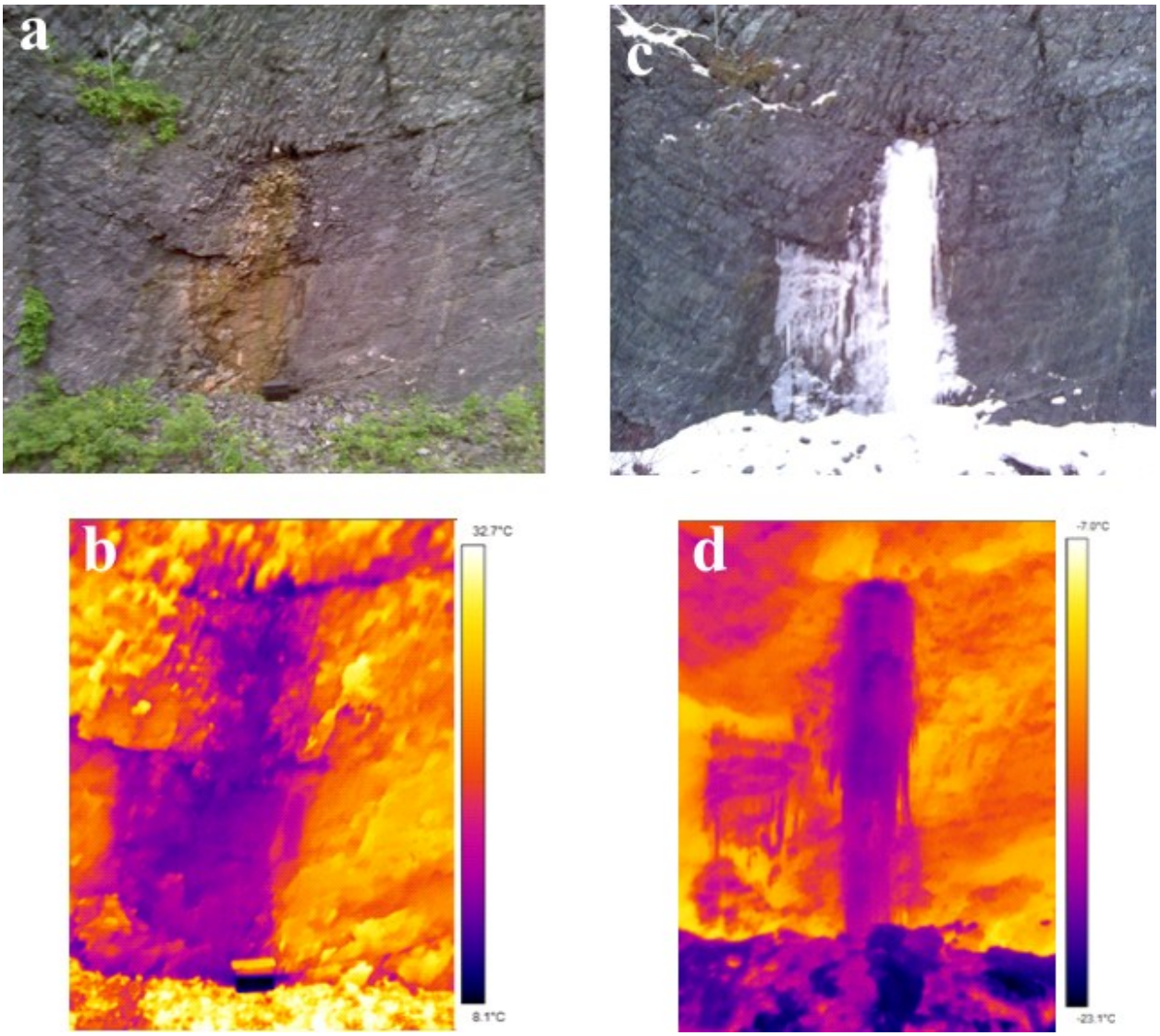

Figure 3. Digital image (a) and thermal image (b) of seep 2-10 taken June 2014. Digital image (c) and thermal image (d) of seep 2-10 taken January 2013**.**

Table 1. Weather conditions during visits to the quarry obtained from nearby weather station.

Date	Temperature (°C)	Humidity (%)	Conditions
21-01-2013	-16	64	Sunny
27-01-2013	-13.1	62	Sunny
14-02-2013	-0.3	75	Cloudy
11-06-2014	17	70	Partly cloudy
11-08-2014	22.8	64	Sunny
10-09-2014	18.5	72	Sunny with cloudy periods
02-10-2014	13	77	Cloudy

During the first quarry visit in January 2013, 55 groundwater seeps were identified. Of these, 31 seeps were readily accessible and selected for analysis. Thermal images and physical observations were recorded for 20 out of the 31 seeps. The remaining 11 seeps had data partially missing because of limited physical access to the seeps, seep absence during some of the field visits, or due to the temporary malfunction of the thermal camera during extreme cold conditions. Herein, each seep is numbered with a two-digit identifier, with the first digit corresponding to the elevation level within the quarry, and the second corresponding to its location on the level, numbered clockwise starting in the north-west corner (Fig. 4 and 5).

During the winter 2013 and June 2014 field visits, thermal and optical images for each seep were collected using a Flir Systems (North Billerica, MA) B300 thermal infrared camera, which measures surface temperature using a 320 x 240 pixel focal plane array and has a spectral range of 7.5 – 13 μm. The thermal and optical images for each seep during the August, September and October 2014 field visits were collected using a Jenoptik VarioCam HD thermal infrared camera, with a pixel resolution of 768 x 1024 and spectral range of 7.5 - 14 μm.). Additionally, if only relative temperatures are used, it is not necessary to correct for emissivity, humidity, and observation distances (Schuetz and Weiler, 2011). Due to these benefits of accuracy and analysis, only relative temperatures were used in the thermal image analyses. The distance between the camera and the base of the seepage face was measured, with an accuracy of 0.5 m, to allow the optical images to be plotted to scale. In addition to the thermal and optical images, physical observations of the seep were also recorded, such as visible flow rate, notable geologic features, and seepage behind the frozen ice seep.

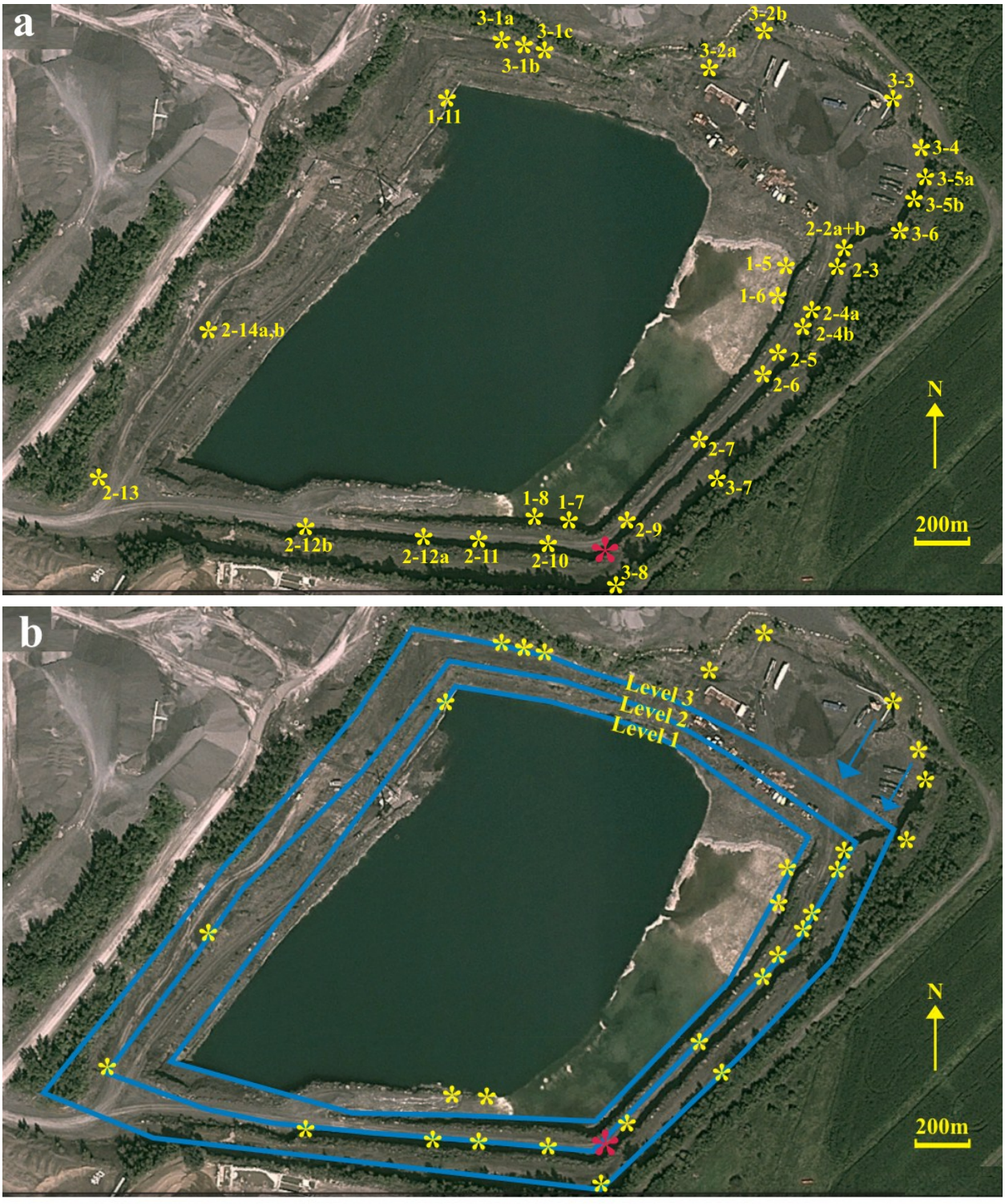

Figure 4. (a) Aerial photo of St. Dominique quarry, with locations of analyzed seeps marked; (b) Aerial photograph highlighting the three elevation levels at the site and the seep locations**.**

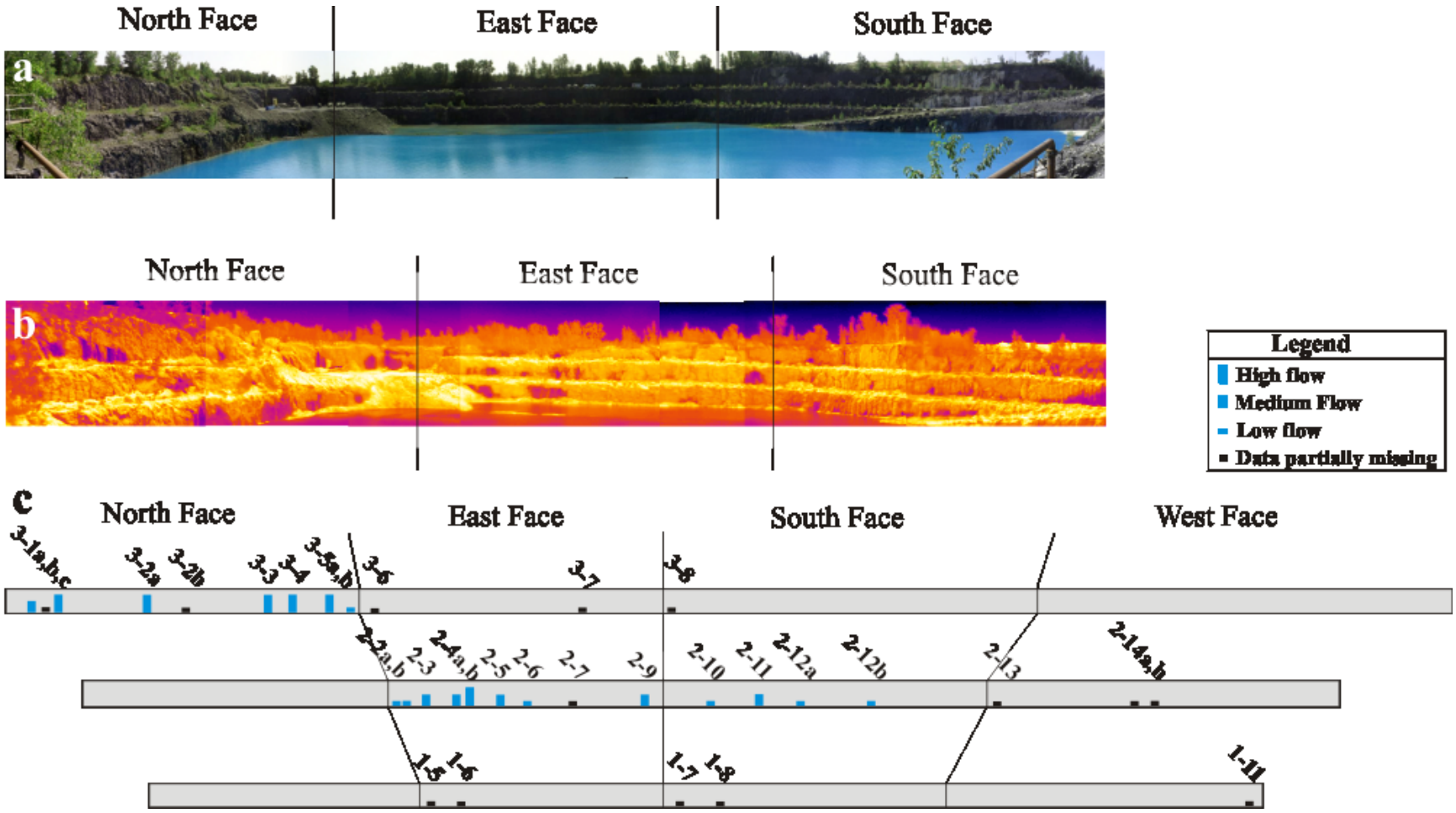

Figure 5. (a) Digital panoramic photograph of St. Dominique quarry; (b) Thermal panoramic photograph of quarry; (c) Scaled seep location and category identification**.**

3.3. Winter observations

Three field visits to the quarry were made during the winter of 2013 (21/01/2013, 27/01/2013, and 14/02/2013). The seeps identified from these visits were categorized as hydraulically active or inactive. Hydraulically active seeps are those that have at least one area of elevated temperature on a thermal photograph, due to groundwater flowing over an exposed surface, or where physical observations indicate that water is flowing behind the exposed ice surface. The area of elevated temperature on a thermal photograph is henceforth called the active zone. The infrared camera only senses the exposed surface, so seeps with groundwater flowing behind the exposed surface cannot be detected using this method (Shea et al., 2012). Seeps are deemed inactive if there is no area of elevated surface temperature on the thermal photograph and no physical observations suggesting flow behind the exposed ice surface.

For the seeps that experienced a period of active groundwater flow throughout the study period, ice formation and degradation was analysed. The optical and thermal images were combined to compare ice growth on optical images and active zones on thermal images. This was completed by resizing and rotating the optical and thermal images from all three trips so as to obtain a consistent scale across all images, which then allowed the percentage change in area of each seep throughout the study period to be calculated (Fig. 6, Table 2). This in turn allowed for the flow in each seep to be estimated. The approximate volume of each seep was multiplied by its percentage change in area between 21/01/2013 and 27/01/2013 and observations of ice thickness, establishing the volume of ice formed in this six-day period. Assuming that the ice thickness was uniform across the seep, and that the flow rate was constant, the flow rate in millimeters per second was calculated (Table 2).

Thermal analysis for each active seep utilized ThermaCAM Research Professional software 2.10 to analyze temperature changes in seep temperatures. A multi-point temperature line was drawn from the top of the active zone to its base. The relative temperature values were plotted against the percentage change in vertical elevation, using the top of the active zone as a reference value for both axes.

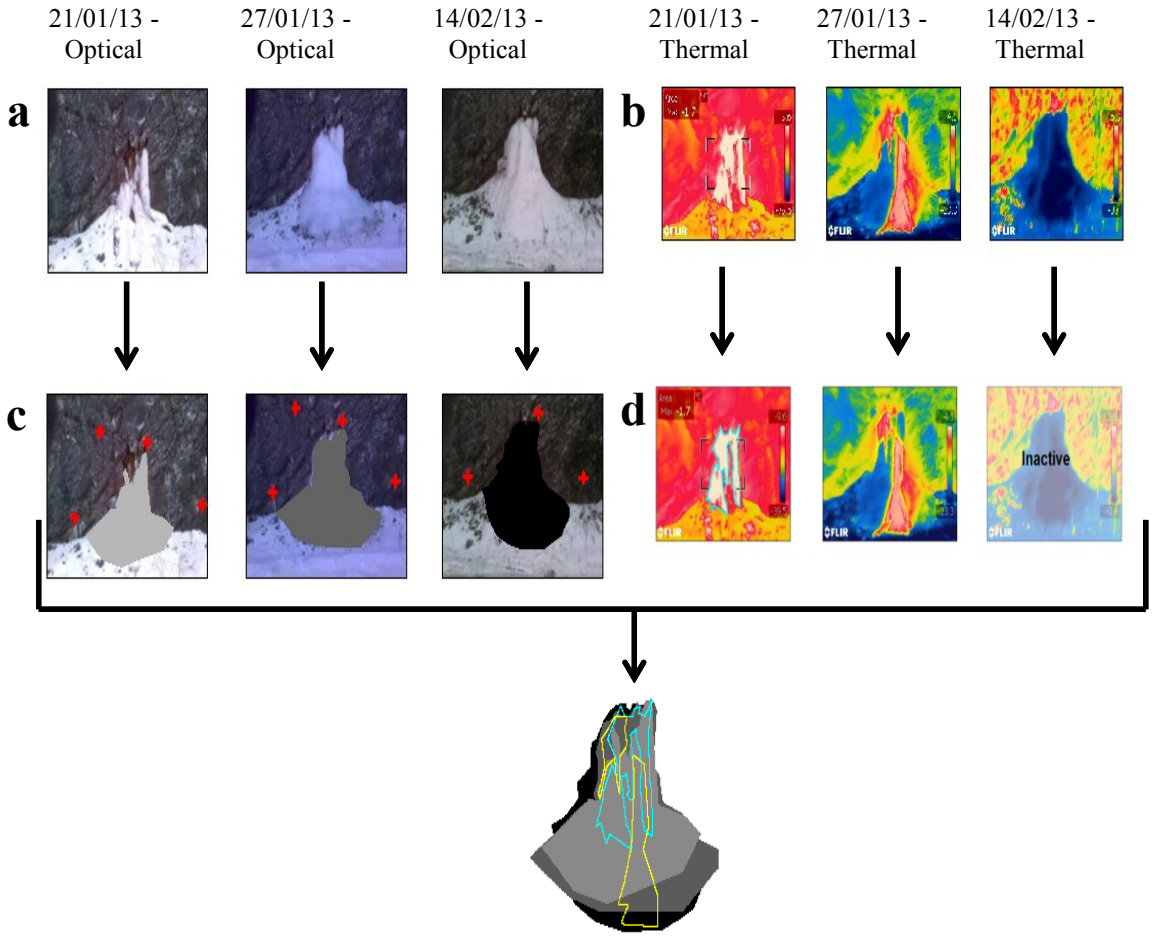

Figure 6. (a) The three photos and corresponding thermal images are imported into AutoCAD. (b) the thermal images are scaled by a factor of 0.83 to match the scale of photographs. (c) A minimum of three match points are added to each photo at identical points. The area of each seep is then identified and hatched in grey. The three optical images are then given a 50% transparency, and superimposed and scaled to match marker points. (d) Lines are drawn around the active zone on each thermal image, and are rescaled to match the scale of the corresponding optical photo. (e) Optical photographs are removed, and lines around active zone added, to produce the final figure.

Table 2. Estimates of volumes and flows of ice seeps.

Seep	% Change in Area 21/01/13-27/01/13	% Change in Area 27/01/13-14/02/13	Approx. ice volume (m^3)	Approximate average flow (ml/second)
2-4a	21	32	5	2
2-4b	52	15	2	2
2-5	12	28	0	0.1
2-6	18	-50	2	1
2-7	-10	-31	2	0
2-9	20	-7	25	10
2-10	22	84	1	0.3
2-11	26	17	10	5
2-14a	65	-8	2	2
2-14b	37	6	2	1
3-1a	53	-42	5	5
3-1b	20	-30	4	2
3-3	40	5	3	3
3-4	40	-3	18	14
3-5	29	-15	103	57
3-7	83	54	4	7

3.4. Summer observations

Three field visits to the field site were made during the summer and fall of 2014 (11/06/2014, 11/08/2014, and 10/09/2014). During each visit, the active seeps were categorized as low flow, medium flow, or high flow. The seeps were categorized by physical observations and crude groundwater discharge estimates. Low flow seeps have no visible flow but possess a wet rock face. Medium flow seeps are those with visible flow of approximately 1 - 4 mL/sec, in the form of slow, singular drips. High flow seeps are those with continuous flow greater than 5 mL/sec.

Thermal analysis for each seep was completed similar to the active seeps in the winter, using the line temperature tool in ThermaCAM Research Professional 2.10 and Jenoptik VarioAnalyzer software. The relative temperature values for each seep plotted against the vertical distance down the seep face are presented in Figure 7. Regression analysis was completed for each seep to develop a function describing the vertical temperature gradient along the cliff face. Fitted lines with R^2 values greater than or equal to 0.8 are considered successful fits.

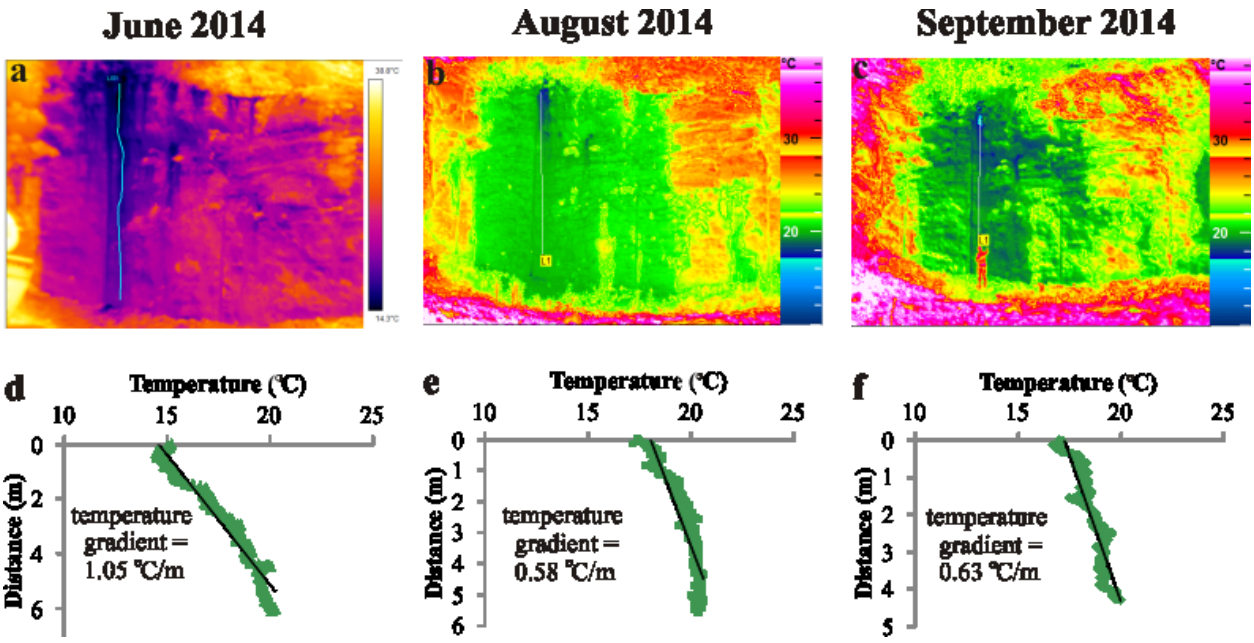

Figure 7. Thermal images and corresponding temperature gradients from June (a, d), August (b, e), and September(c, f) (2014) for Seep 3-5. A temperature line profile was recorded down the quarry cliff face using the thermal imaging program ThermaCAM Researcher Professional 2.10 and VarioAnalyze Pro, respectively. This was then plotted against the distance down the cliff face to determine the temperature gradient.

3.4.1. Time-lapse thermal imagery

Twenty-four hours of time-lapse thermal imagery was captured on two seeps in August 2014 to evaluate the role of changing air temperature and solar radiation. Deitchman and Loehide (2009) showed that time-lapse thermal imagery was useful in determining the optimal time to utilize thermal imagery to distinguish the location of the water table from a drainage ditch seepage face, and therefore was the motivation behind this experiment. Additionally, observations over a 24-hour period allow for explicit observation of the effects of diurnal solar radiation and the response of rock and water to changes in atmospheric temperature. South-facing Seeps 3-1a and 3-1c were chosen for this experiment because they represented a medium and high flow rate, with the hypothesis that the contrast between these seep types would best demonstrate the relationship between groundwater discharge and rate of groundwater warming down a cliff face. Thermal and optical images were captured every half hour throughout the duration of the test.

3.4.2. Artificial seep experiment

A controlled artificial seep experiment using two constant head tanks was performed at the quarry in October 2014 to examine the vertical temperature gradient when the discharge rate was known precisely. Two large constant head tanks filled with water (~10 °C) were placed on the third level of the east face of the quarry (Fig. 4). This location in the quarry was chosen for its fractured, relatively homogeneous cliff-face, with no visible seeps nearby to alter or affect the experiment. Tubing from each head tank was placed onto the cliff face of the second quarry level. Water was discharged from the head tanks at a rate of 1.5mL/sec and 5mL/sec, representing medium and high flow rates, respectively. Thermal images of the artificial seeps were collected every half hour for eight hours.

3.5. Results

3.5.1. General observations of seeps

The location of seep origins were consistent throughout the study period, but the size, appearance, and thermal profile of the seeps changed over time scales ranging from hours to days. The majority of the groundwater seeps evolved throughout the study period by expanding or sometimes contracting laterally from a singular seep source, originating from a single flow source in the fractured rock. The seeps formed along a well-defined fracture on a bedding plane, or at a localized independent fracture intersection. Future analysis of the local geology may determine a relationship between geological features and groundwater seep formation.

The apparent hydraulic activity of the seeps decreased in both the winter and summer study period on a weekly time scale. In winter, there was an observed reduction in the number of active zones identified on the second and third visits. Of those active on the first trip, 30% were inactive by the second, with only one thermally active seep on the third visit, which suggests that extreme cold temperatures can freeze the seep origin at the fractured bedrock face. Despite the apparent decrease in hydraulic activity in the winter study period, there was an average increase in the visible ice area of 33% between the first and second visits. Between the second and third visit, due to a period of above freezing temperatures, 50% of ice seeps decreased in size. In the summer, the groundwater seepage rates reduced significantly between the June and August visits. Eighty percent of the seeps categorized in June as low flow had no visible flow in August

and September. Similarly, 40% of the seeps categorized as medium and high flow in June were reduced to low flow seeps in August and September, correlating to the drier part of the summer.

The location of the active zone on the frozen groundwater seeps did not remain constant throughout the study period. The majority of the active zones were located at the edges of the frozen seeps. This suggests that most frozen seeps predominantly develop laterally across the cliff face as vertical channels, rather than perpendicular to the cliff face (although this must happen too since the frozen seeps are 10 cm to >2 m thick). There was also a clear relationship between zones identified as thermally active, and areas of ice growth on the following visit. For example, the first visit in January 2013 showed four areas of active flow for seep 2-14a. The seep was found to have expanded directly below two of these on the second visit. There was only one active zone on the second visit, and the final visit found that this was the only area where ice expanded.

3.5.2. Thermal analysis

The relative temperature analysis of the frozen groundwater seeps does not show a clear trend in change in groundwater temperature with distance from top of the active zone. For most seeps, groundwater flow did not cool appreciably along the cliff face (Fig. 8). This contrasts the results of Pandey et al., (2013), where two distinct thermal zones on the active ice surface were observed, with appreciable and consistent cooling with vertical distance from the seep origin. The relative temperature analysis of the groundwater seeps during the summer study period did show a qualitative relationship between groundwater discharge at the seepage face and rate of groundwater warming down a cliff face (Fig. 9). The vertical temperature gradient, which represents the change in groundwater temperature with vertical distance from the seep origin, is generally lower in seeps with higher flow, such as seep 3-5, suggesting that groundwater did not appreciably warm down the rock face. This can be compared to seep 2-9, a much lower flow, which had a much higher vertical temperature gradient, meaning appreciable warming down the rock face. Vertical temperature gradients for medium and low flows were not as easily distinguishable, as both possessed fairly high temperature gradients, indicating appreciable warming down the rock face.

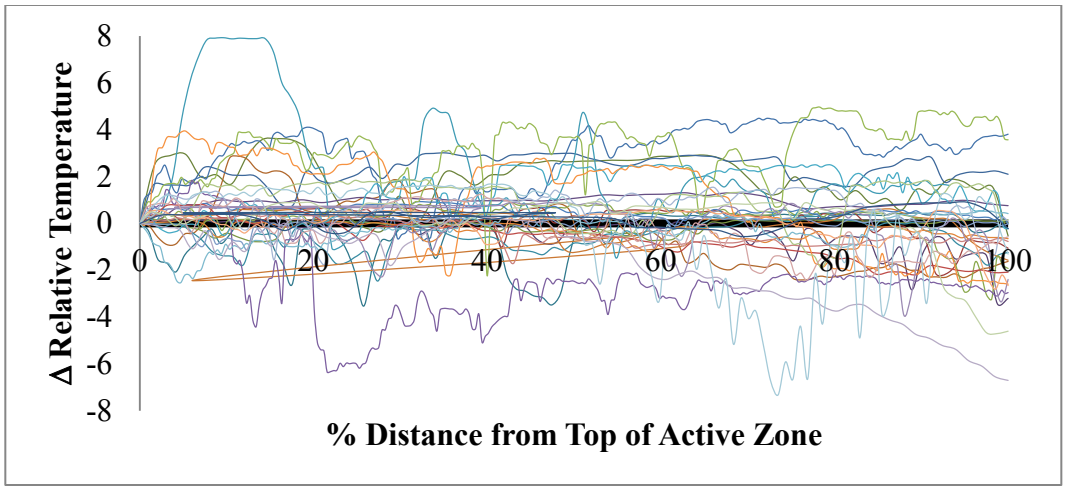

Figure 8. Change in relative temperature between top and bottom of active zone for each seep during winter conditions.

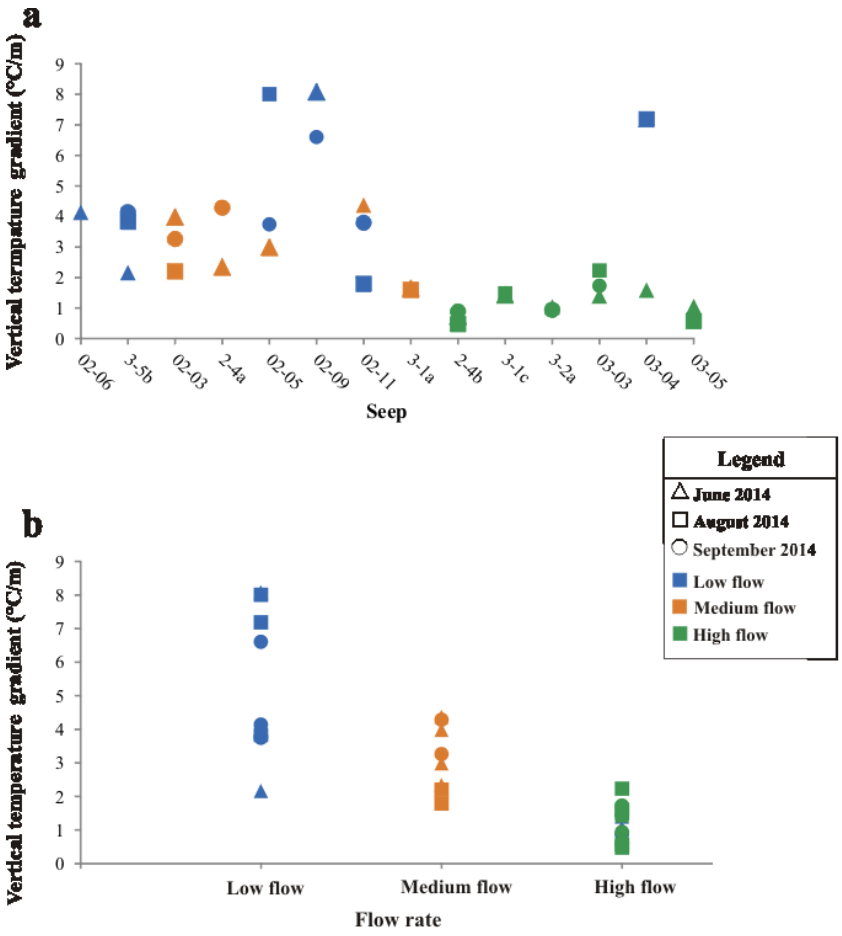

Figure 9. (a) Temperature gradient for all seeps from June – September 2014. (b) Temperature gradient compared to flow rate. The low and medium flow seeps generally have higher temperature gradients (ie. more warming) as compared to higher flow seeps, which have lower temperature gradients (ie. less warming).

3.5.3. Time-lapse thermal imagery

Time-lapse thermal imagery of seeps 3-1a and 3-1c during the summer period indicates that the relationship between groundwater discharge at the seepage face and vertical temperature gradient can change on a daily time scale as well (Fig. 10). The vertical temperature gradient decreases by as much as three times as the night progresses, indicating there is less warming of the groundwater as it flows down the cliff face due to the cooler ambient air temperatures. Around 6:00 am, when the sun rises, the vertical temperature gradient increases. This is most likely due to the increase in ambient air temperature, which warms the cliff face and groundwater seepage, resulting in a higher temperature gradient, and a more appreciable warming of groundwater down the cliff face. Throughout the day, this pattern continues, as the vertical temperature gradient becomes noticeably higher, meaning more warming of the groundwater as it flows along the cliff face. From 10:30 am until 4:00 pm, the cliff face was in direct sunlight. The presence of solar radiation, as well as higher air temperature, increased the temperature gradient. Around 6:00 pm, as air temperature and solar radiation decreased, the temperature gradient begins to lower again, similar to the temperature gradient of the previous day. This pattern is apparent in both seeps.

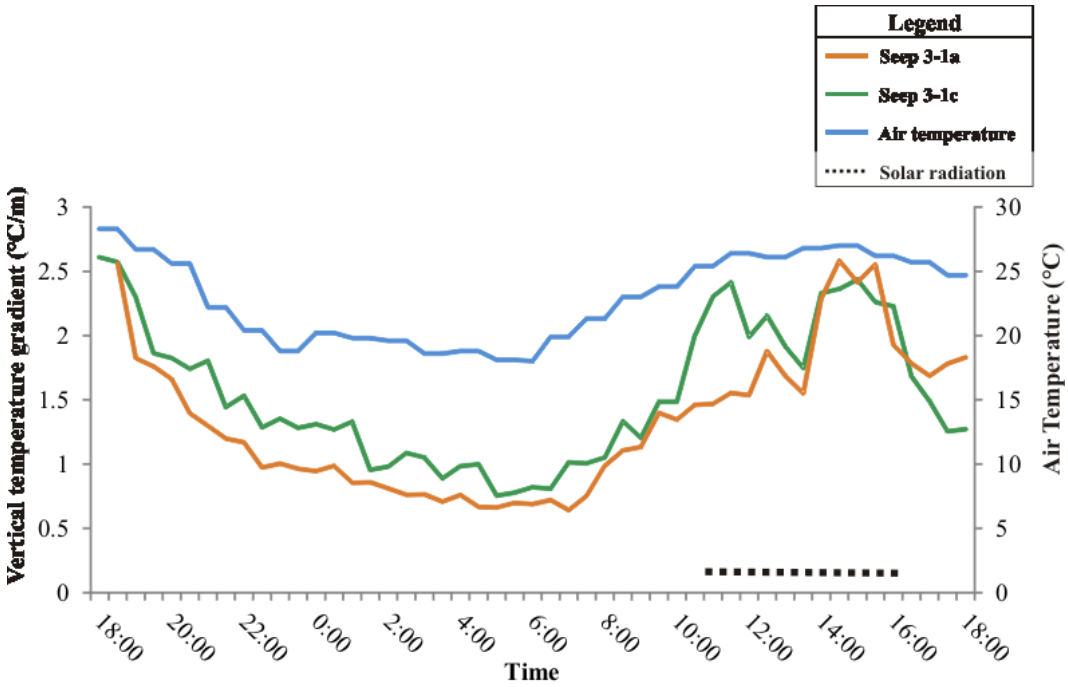

Figure 10. Temperature gradient results from the 24-hour time-lapse thermal imagery of Seep 3-1a and 3-1c. The temperature gradient is lowest in the night (i.e. less warming) and higher during the day (i.e. more appreciable warming).

3.5.4. Artificial seep experiment

The controlled artificial seep experiment produced vertical temperature gradients slightly larger than the natural groundwater seeps found within the quarry (Fig. 11a). The temperature gradients for the medium and high flows were reasonably consistent throughout the experiment, meaning although the magnitude of the temperature gradients were not as low as expected, they are consistent with the above qualitative relationship between temperature gradients and seepage flow rates. The vertical temperature gradients may be larger than the natural seeps because the experiment was completed for only 8 hours, so the artificial seeps may not have had enough time to mature and emulate the nature of the authentic seeps in the field. Additionally, fractures and small complexities in the cliff face redirected and modified the flow (Fig. 11b and c). Instead of flowing vertically down the cliff face, the water seeped into the cliff face and flowed horizontally along fractures. This complicated the ability to accurately capture vertical temperature gradients. However, qualitatively, this experiment shows that higher flows have lower temperature gradients throughout the day, meaning less appreciable warming down the rock face, as compared to lower flows.

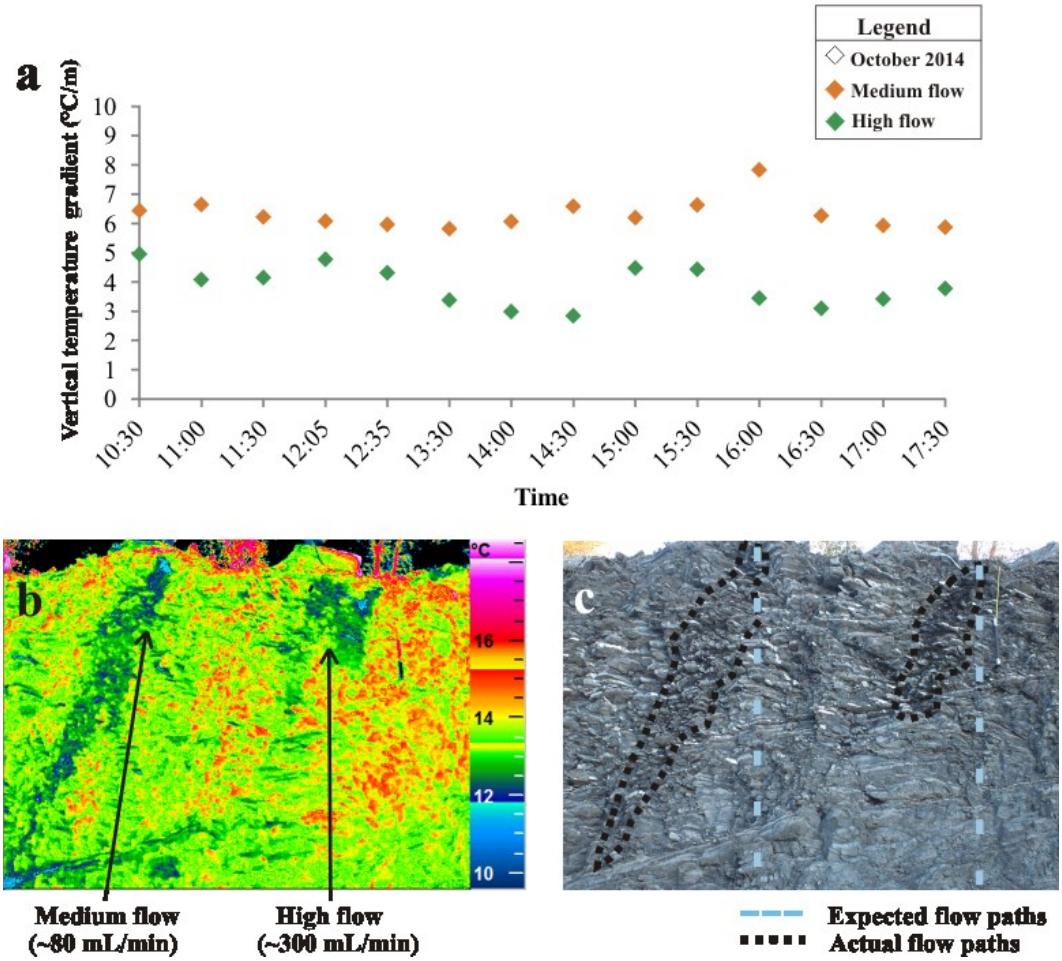

Figure 11. (a) Vertical temperature gradient observed from the artificial seep experiment in October 2014 for medium and high flow. Qualitatively, the medium flow seep has a higher temperature gradient (ie. gradual warming), as compared to the higher flow seep (ie. low temperature gradient, less warming); (b) Thermal photograph showing altered flow paths from cliff complexities; (c) Optical photograph showing the geology of the cliff face, with expected and actual flow paths.

3.6. Possibilities for the thermal imagery of groundwater seeps

3.6.1. Locate and qualitatively characterize seeps

Thermal imagery is a non-invasive technique that is effective at locating and qualitatively characterizing groundwater seeps (Loehide and Gorelick, 2006; Waldick and Conant, 2006; Deitchman and Loehide, 2009; Pfister et al., 2010). We add to this growing field of research with a systematic study over one year, using a vertical temperature gradient to qualitatively characterize groundwater seeps. During the winter, thermal imagery can be used to locate areas of active groundwater flow in frozen seeps, which can allow for areas of ice growth to be

predicted. Combined with optical images, rates of ice growth can be estimated from thermal images, which can offer insight into groundwater flow patterns through fractured rock and discharge at the seepage face. In the summer, thermal imagery can be used to qualitatively differentiate between low and high flow seeps, using a temperature gradient down the vertical cliff face. Higher flow seeps generally have lower temperature gradient, meaning less appreciable warming down the cliff face, as compared to lower flows. Additionally, thermal imagery is effective at locating low flow seeps that might have otherwise gone unnoticed.

The results obtained from this study provide direction for future research using thermal imagery to characterize groundwater seepage flux. Future research should focus on time-lapse thermal imagery of groundwater seeps in order to fully understand the diurnal temperature gradients observed in this study. Time-lapse thermal imagery should be taken at different times throughout the year to see if the diurnal gradients are consistent, or if they are not, how they change throughout the year. Detailed discharge measurements, taken at the seep source, should be taken in addition time-lapse thermal imagery. This may help determine a quantitative relationship between groundwater discharge and thermal gradients. This relationship can be further tested by additional artificial "seep" experiments possibly for longer durations to ensure the artificial seeps are steady-state.

3.7. Limitations of the thermal imagery of groundwater seeps

3.7.1. Significant temperature differential between air and groundwater required

Thermal imagery is most effective at locating seeps when the temperature differential between groundwater and the ambient air temperature is large. During the third winter visit, thermal imagery identified only one seep to be active. However, visual observations established that in fact 8 seeps remained active. This is because the temperature of groundwater was 0.1 °C, making the temperature differential between groundwater and ambient air temperature too small for thermal imagery to detect groundwater flow. Therefore, the efficacy of thermal imagery to locate and characterize seeps is limited to areas with strongly seasonal climates when the air temperature and groundwater temperature are significantly different.

3.7.2. Cliff face heterogeneity affects thermal gradients

The artificial seep experiment showed that small complexities in the fractured cliff face topography redirected and modified flow. When flow is redirected such that it no longer travels vertically towards the surface, which is possible even on moderately rough cliff faces that appear relatively homogenous, the measurement and analysis of vertical temperature gradients is compromised, as the technique inherently requires warming along a vertical flow path. In the artificial seep experiment, the artificial seeps did not flow vertically down the cliff face, as required. Instead, the water seeped into the cliff face (along the dip of the rocks) and flowed horizontally along fractures. It is possible that the seeps show more warming, and therefore larger temperature gradients, because the water is actually flowing into the rock face (along the dip of the rocks), rather than vertically down the cliff face. This applies for natural seeps too, as fractured cliff faces are complex and surface flow paths are difficult to predict a priori. This may contribute to the overlap between low, medium and high flow temperature gradients.

3.7.3. Frozen seeps are complex with no consistent thermal gradients

Frozen seeps observed in the winter were significantly different from the findings of Pandey et al. (2013), where two distinct thermal zones on the active ice surface were observed, with appreciable cooling along the seepage face. The experiments conducted by Pandey et al. (2013) were completed in a controlled laboratory setting which resulted in two distinct thermal zones and consistent cooling along the 'seepage face'. The thermal conductivity of ice and rocks are much less than that of the constructed design (e.g. metal sheets) used by Pandey et al. (2013). The flat metal sheet roughened with glued sand used in the experiments also greatly differs from the complexity of fractured rocks in the field. Additionally, unlike the frozen seeps created by Pandey et al. (2013), the majority of the active zones within the frozen seeps at the quarry were at the edges of seeps. Finally, the seeps simulated in Pandey et al. (2013) were immature, generated on a much smaller time scale than the seeps studied in the quarry. As such, the artificial seeps may not have had enough time to mature and emulate the nature of the seeps in the field. In the field, the lack of a clear trend in change in temperature with distance from the top of the active zone suggests that most seeps predominantly develop as vertical channels that migrate laterally across the ice face, and sometimes flow beneath the surface. The lack of observed thermal breaks or gradients in field observations suggest the breakpoint analysis used

in Pandey et al. (2013) to determine the two thermal zones was not suitable for the field observations. In sum, it seems that even qualitative relationships between discharge rate and temperature gradient are unlikely during winter conditions, suggesting that summer conditions may be more appropriate to focus future efforts on.

3.7.4. Temperature gradients vary diurnally

The observations from the 24-hour time-lapse experiment indicate that time-series thermal imagery, as opposed to a single image in time, is essential for characterizing seepage faces. Individual thermal images can be unrepresentative of the mean temperature gradient for the seep, depending on the time of day the image was captured. The temperature gradient becomes lower as the night progresses and is higher throughout the day, indicating there is less warming of the groundwater as it flows down the cliff face throughout the night as compared to the warming throughout the day. Future work should focus on determining the optimal time to utilize thermal imagery to capture representative vertical temperature gradients.

3.7.5. Thermal cameras have limitations

It is important to consider the limitations of thermal cameras themselves. Absolute temperatures from thermal cameras must be corrected for emissivity, humidity and observation distances in order to have robust, quantifiable data (Aubry-Wake et al., 2015*)*. Changing atmospheric conditions, reflected radiation, and observation angles are a just few of parameters that can affect thermal images. Aubry-Wake et al. (2015) discovered that changing atmospheric conditions (i.e. overcast, passing clouds) can affect the measured thermal imagery data in high-altitude alpine environments, and are not easily corrected for. Cardenas et al. (2008) noted that radiation emitted from personnel near their area of study resulted in the detection of anomalous sources of radiation in their thermal imagery. Therefore, appropriate framing of the area being captured is important to reduce the amount of reflected radiation. Proper framing must also ensure that the observation angle from the object is less than 45° from the perpendicular, as anything beyond this will affect the emissivity and impact affect the thermal image (Vollmer and Möllmann, 2010). Additionally, water surface roughness (wind) and turbidity produces an irregular incident angle, which affects emissivity and can have an effect on the temperature patterns recorded in the thermal image (Liu et al., 1987; Masuda et al., 1988; Hare et al., 2015).

A more detailed description of the limitations of thermal imagery can be found in Vollmer and Möllmann (2010). In sum, these complications, if present, must be carefully addressed in order to ensure the thermal signatures captured from a thermal image are correct. Our analysis of thermal images used relative temperature, as it was deemed more accurate than absolute temperatures and avoids the need to correct for emissivity, humidity, and observation distances. .

3.8. Conclusions

Thermal imagery of groundwater seeps in an unused fractured rock quarry was captured over a 22 month period to determine the efficacy of thermal imagery for quantifying groundwater discharge at seepage faces. The seeps evolved over short periods of time, changing in size, appearance and thermal profile. Thermal imagery was effective at locating and qualitatively characterizing seeps. During the winter, areas of active groundwater flow and ice growth can be predicted from thermal images, as well as crude groundwater flux estimates. During the summer, thermal images can be used to qualitatively differentiate between low and high flow seeps, using a temperature gradient from the seep source down the vertical cliff face. Higher flows will have a lower temperature gradient, suggesting less appreciable warming down the cliff face, as compared to lower flows.

Thermal imagery has several limtiations in characterizing groundwater seeps. A robust quantitative relationship between groundwater discharge and the temperature gradient down the vertical cliff face could not be determined using thermal imagery, due to complexities in the fractured rock cliff topography that alter and modify flow paths, and temperature gradient changes throughout the day. However, future work with time-series thermal imagery of groundwater seeps may be able to determine a relationship between the changing temperature gradient and groundwater discharge at the seepage face.

Despite the limitations discussed above, thermal imagery is effective at locating and qualitatively characterizing groundwater flux at the seepage face. The results from this study provide insight into the current limitations thermal imagery has in quantifying groundwater discharge at the seepage face, and provides direction on what options to pursue in the future.

Chapter 4. Complexity of hydrogeologic regime around an ancient low-angle thrust fault revealed by multi-disciplinary field study

4.1. Introduction

Fault zones in the upper crust are known to have a dominant impact on numerous hydrologic processes. Fault zones can affect regional groundwater flow (Mayer et al., 2007; Bense et al., 2008; Burbey, 2008; Kim et al. 2014), hydrothermal fluid circulation (Berkowitz, 2002; Faulkner et al., 2010), carbon sequestration (Shipton et al., 2004; Agosta et al., 2008), emplacement of petroleum resources (Aydin, 2000; Sorkhabi and Tsuji, 2005), and affect the storage of nuclear waste (Bredehoeft, 1997; Douglas et al., 2000). Although fault zones have been extensively studied and conceptual models developed for various geologic settings, the permeability architecture and fluid flow paths of fault zones remain hard to constrain and predict *a priori*. This is because the hydraulic properties of fault zones vary greatly depending on the lithology of the host rock, fault displacement, geologic setting, state of stress, and temporal evolution of the fault (Smith et al., 1991; Scholz and Anders, 1994; Caine et al., 1996; Lopez and Smith, 1996; Bense et al., 2013). Moreover, fault components are heterogeneous and anisotropic, with varying permeability temporally and spatially (Faulkner et. al., 2010).

Faults in carbonate rocks exhibit a broad range of hydrogeologic behaviors; from effective conduits due to dissolution weathering, dilatational jogs, and uncemented fracture networks (Andrews et al., 1982; Billi et al., 2007; Bense et al., 2013), to significant barriers due to smearing of low permeability material (e.g. clay gouge) into the fault core (Agosta and Kirschner, 2003; Doan and Cornet, 2007), secondary cementation (Micarelli et al., 2006), or the formation of fine-grained cataclastic fault rocks (Agosta and Kirschner, 2003; Celico et al., 2006). Additionally, combined of conduit-barrier systems have been recorded in carbonate rock faults (Allen and Michel, 1999, Breesch et al., 2009).

Research on fault zone hydrogeology is often hindered by a lack of synergy between structural geologists and hydrogeologists. Both aim to characterize fluid flow around fault zones, yet the two disciplines concentrate on different field areas and use diverse methods that integrate over different scales (Bense et al., 2013). Structural geologists often focus on surface studies, investigating outcrops that can scale up to hundreds of meters, or analyzing rock samples.

Hydrogeologists usually focus on subsurface data, using pumping tests, geochemical surveys, and geophysical data from wells and springs to determine aquifer parameters on local to regional scale (Bense et al., 2013). Well-exposed fault zones in outcrop are generally located in areas where a dense network of wells needed for hydrogeologic investigations is not feasible, as these areas are less developed. However, well networks are seldom where we need them and are predominately placed in well-developed areas, where well-exposed outcrops needed for structural geology measurements are sparse (Bense et al., 2013).

The remarkable exposure of the Champlain Thrust fault at the edge of Lake Champlain at Lone Rock Point in Burlington, Vermont, allows for both structural and hydrogeologic field observations, providing direct data about the lithology, architecture, and hydrogeology of the fault. The Champlain Thrust fault is a surface expression of the frontal thrust of the Taconic Orogeny, which emplaced the Lower Cambrian Dunham dolostone over the Middle Ordovician Iberville shale (Rowley and Kidd, 1980; Stanley, 1987; Hayman and Kidd, 2002). The hydrogeology of the Champlain Thrust has never been studied before, and thus represents a unique opportunity to report on the hydrogeology of thrust faults in carbonate settings where mechanically distinct units are juxtaposed.

The objective of this paper is to establish a preliminary understanding of the hydrogeology a low angle thrust in sedimentary rocks, using a multi-disciplinary approach. We describe the prominent structural features of the Champlain Thrust fault at the Lone Rock Point outcrop. Hydrogeologic observations from groundwater seeps exposed along the outcrop are presented and related to the structural features in an attempt to establish a correspondence between fault structure and groundwater flow. Aquifer pumping tests in the hanging wall and fault are interpreted from two wells drilled near the outcrop. Rock core was obtained from one of these wells to complement the outcrop structural analysis.

4.2. Champlain Thrust

The Champlain Thrust fault extends from southeastern Quebec to the Catskill Plateau in east-central New York (Stanley and Ratcliffe, 1983, 1985; Rowley, 1983; Ratcliffe et al., 2011). It is the southern extension of the larger Logan Line thrust system marking the frontal thrust of the Taconian Orogeny of Middle to Late Ordovician age (Fig. 12; Rowley and Kidd, 1980; Stanley, 1987; Hayman and Kidd, 2002). North of Burlington, USA, the orientation of the Champlain Thrust fault is relatively consistent, striking north and dipping approximately 15

degrees eastward. South of Burlington, the fault has been deformed by high angle faults and broad folds, making the trace irregular. The displacement along the Champlain Thrust fault is estimated to be 60 – 80 km, along an azimuth of approximately N60°W (Stanley, 1987).

The fault is exposed on the shore of Lake Champlain over a roughly 1 km long segment at Lone Rock Point, Burlington, Vermont (Stanley, 1987) (Fig. 12). Here, the thrust strikes north-northwest and dips shallowly to moderately to the east. The fault juxtaposes the Lower Cambrian Dunham Fm. (hanging wall) over the Middle Ordovician Iberville Fm (footwall). The throw is estimated to be 2,700 m by stratigraphic constraints (Stanley, 1987). Contrasts in erosional competencies cause the hanging wall to be undercut by lake erosion (Stanley, 1987).

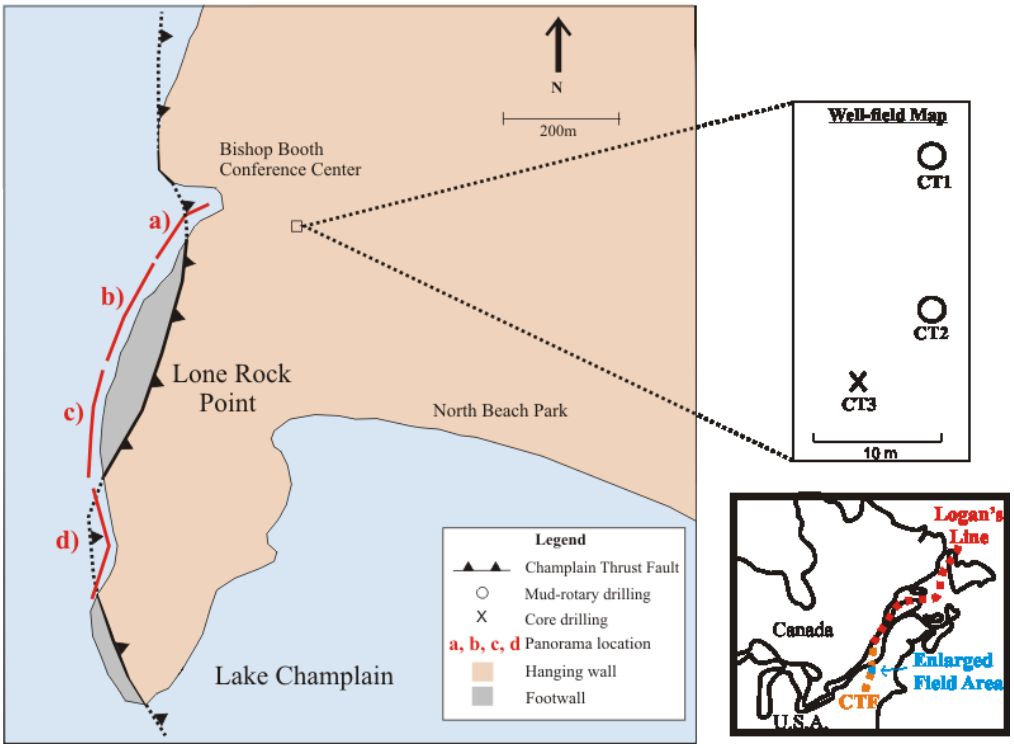

Figure 12. Location of Champlain thrust fault (CTF) and well placement. Location of panorama (Fig. 13) outlined in red.

4.3. Fault geometry from outcrop

We mapped the outcrop of the Champlain Thrust at Lone Rock Point on panoramic photos taken from the frozen lake (Fig. 13), and recorded the lithologic and orientation characteristics of the fault surface along ~700 m of strike section. We documented the structural style of the fault, especially focused on changes in width, orientation, or character of the fault

rock along strike. We sampled the fault rock, hanging wall and footwall rock, to determine the microstructure by optical petrography and mineralogy by bulk powder X-ray diffraction (XRD).

The hanging wall is beige crystalline dolostone of the Dunham Fm., crosscut by open fractures, and calcite and dolomite veins. The footwall marly shale of the Iberville Fm. is pervasively folded and crosscut by joints and veins in the vicinity of the Champlain Thrust. Bedding is ~1-3 cm-thick, alternating massive fine-grained limestone and dark gray to black marly shale, cut by white calcite veins which are most abundant in fold hinge zones. The folds in the footwall shale are typically tight to isoclinal, shallowly plunging with shallowly dipping axial planes. The footwall is cut by brittle faults in diverse orientations, most of which do not cut across the fault into the hanging wall. X-ray diffraction shows that the hanging wall dolostone is >90% dolomite with a few % each quartz and illite, while the footwall contains ~ 75% calcite, 15% quartz, and 10% illite and other phyllosilicates.

The fault core of the Champlain Thrust includes is a zone of deformed fault rock which contains a mixture of hanging wall and footwall components, calcite and dolomite veins, and brecciated/reworked vein fragments. The contacts between fault rock and the hanging and footwall are sharp and undulating. The color varies from black to gray to beige, and is locally massive within lenses of breccia, and locally foliated with asymmetric S-C fabric. Mineralogy of the fault rock, as determined by XRD, shows variable proportions of dolomite, calcite, quartz, illite and other phyllosilicates. The source of dolomite to the fault rock is comminuted hanging wall dolostone. Calcite, quartz, and illite are sourced from comminution of footwall marls. In some cases, we observe an increase in calcite proportion within fault rock that is not coupled with increased quartz and illite. This likely indicates that the calcite was introduced as veins and cements rather than fragments of footwall rock.

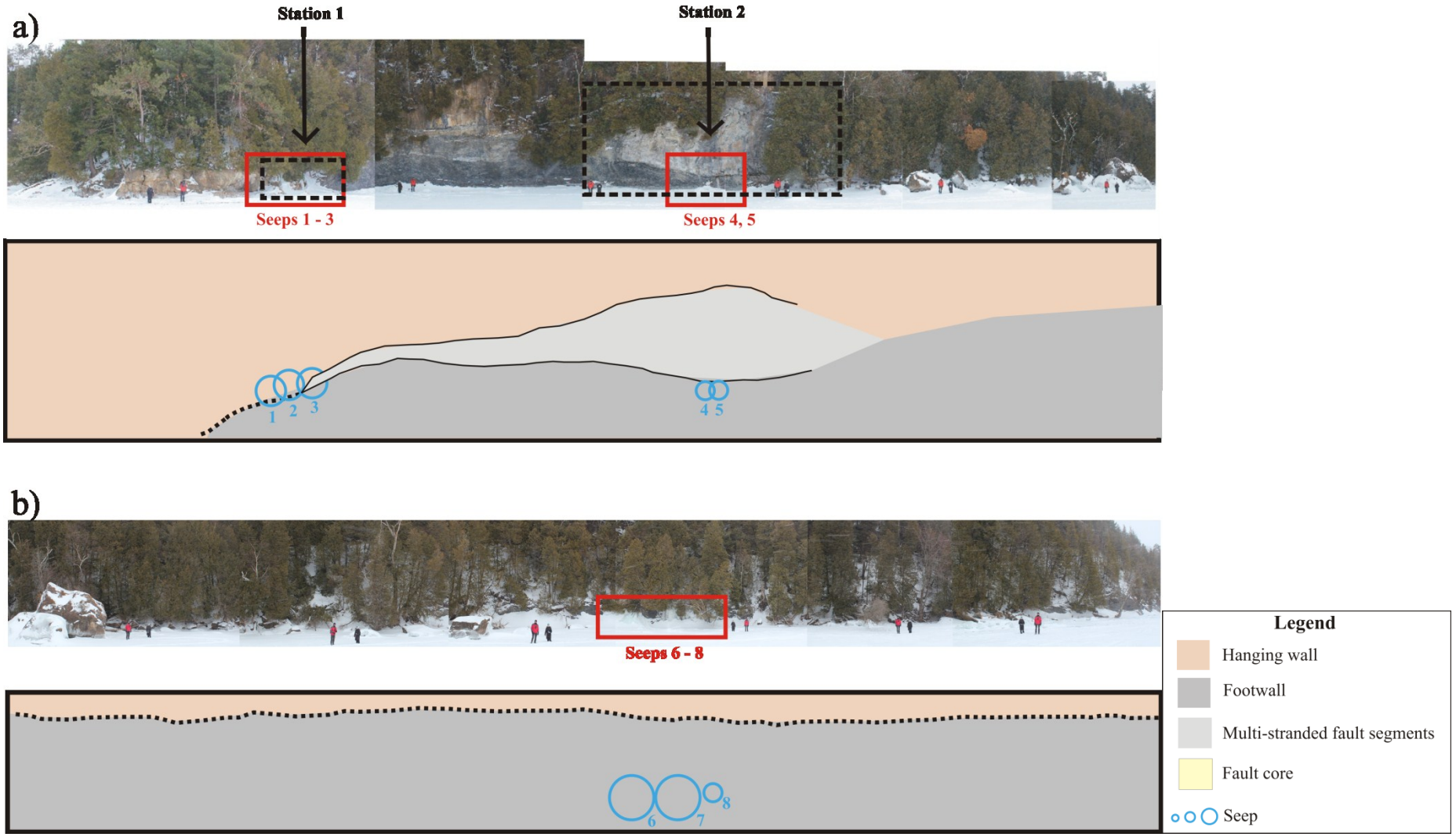
a)
Station 1
Station 2
Seeps 1 - 3
Seeps 4, 5
1 2 3
4 5
b)
Seeps 6 - 8
6 7 8
Legend
Hanging wall
Footwall
Multi-stranded fault segments
Fault core
Seep

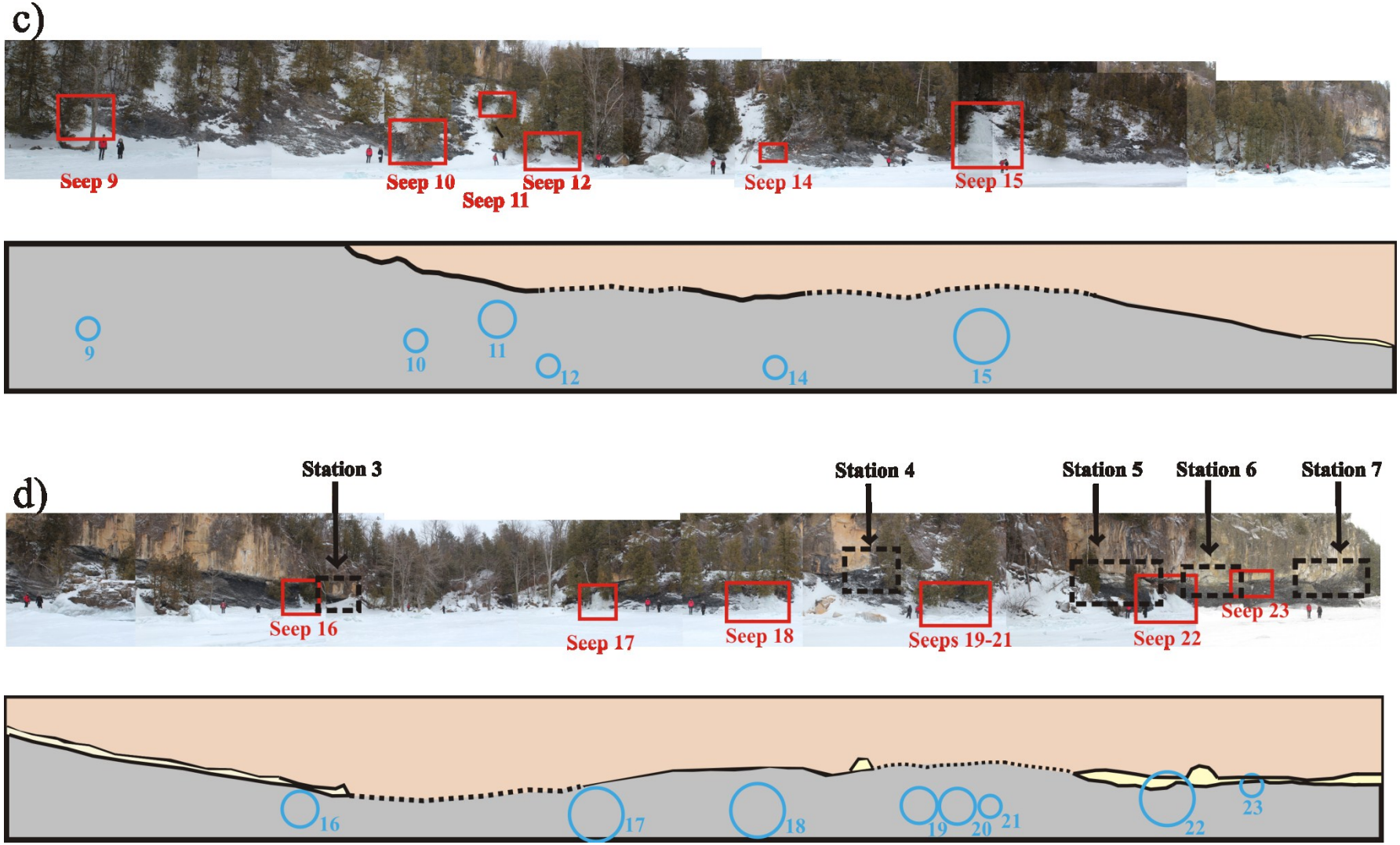

Figure 13. Panorama of the Champlain Thrust fault. The panorama was shot from the frozen lake surface, from north (a) to south (d). Areas with prominent structural features are outlined in black, and frozen seeps locations are outlined in red (See Fig. 12 for placement on map). Scaled circles represent the small, medium, and large flows observed from the frozen seeps, with the number corresponding to seep number. Scale is defined by people at the base of the fault. Total length of panorama is is ~700 m.

The fault core normally consists of 0.1-0.4 m of fault rock, and one sharp continuous fracture surface, interpreted as the principal slip surface. The principal slip surface usually divides the hanging wall from the fault core, but locally where the fault rock thickens, the principle slip surface crosscuts the fault rock (older breccias and foliated cataclasites) before rejoining the hanging wall interface. The average principal slip surface plane is oriented 017°/11°E, with variations of ~ 16° in strike and ~4° in dip corresponding to the meter-scale corrugations on the hanging wall surface (n=27). Based on the crosscutting relationship with other rocks of the fault core, we interpret this discrete surface as likely the latest surface of active slip in the Champlain Thrust.

Several steep normal faults of displacements <10 m, and a few of displacements >10 m, postdate and offset the Champlain Thrust. These faults contain angular fault breccias partially cemented by porous chalky calcite, and are readily distinguishable in outcrop and in fault core from the original Champlain Thrust fault rocks.

At the northern exposure of the Champlain Thrust fault, the main fault splays out into a chaotic network of synthetic faults in a zone roughly 3 m thick in the north, increasing to 8 m thick over a ~30 m long segment of the fault (station 2, Fig. 13; Fig.14b), herein referred to as 'multi-stranded fault segments'. The southern along-strike transition from a discrete fault surface to the south into this complex multi-stranded segment is not exposed. To the north, the Champlain Thrust fault is cut by a normal fault and down-dropped below lake level (station 1, Fig. 13). The normal fault surface is stepped, striking 306° with dips ranging from 50° to 89°. The fault rock between slip surfaces of the splays is texturally diverse. Large imbricate lens-shaped blocks of fault rock, isolated by bounding synthetic faults, weather dark to pale grey.

Steep-walled embayments filled with older fault rock occur in the hanging wall dolostone directly above the principal slip surface, which truncates them. These are variably sized (20-40 cm wide by 20-40 cm thick) and composed of cohesive cataclasite (station 3 - station 6, Fig. 13, Fig. 14d). On fresh surfaces, it is possible to distinguish variably-sized (<5 cm), randomly oriented clasts in a dark blue crystalline matrix. These occurrences of relict fault rock preserved in hanging wall embayments were only observed on sections of the fault where the hanging wall had recently collapsed, exposing large fresh surfaces above the fault. Mineralogy determined by XRD shows that calcite is enriched in these healed breccias, indicating that dolostone fragments were cemented by calcite veins during fault rock healing.

Three areas of the exposure show localized abrupt thickening of the fault rock (station 3, station 6, station 7, Fig. 13; Fig. 14c), accommodated by concavities in the hanging wall surface. The fault core in station 7 (Fig. 13) reaches up to 3 m thick. The best-exposed example is at station 6 (Fig. 13). The fault rock thickens to more than 2.5 m over 3 m in strike length. The geometry of the thickened section is asymmetric; the left side dips steeply into the main fracture, while the right side tapers into it. The principal slip surface cuts through the middle of the thickened fault rock. The southernmost recorded occurrence of a thickened section of the fault core is at station 3 (Fig. 13). Here, the fault rock thickens to ~0.5 m over a 2 m segment of the fault. The transition from normal fault core thickness to the thickened section is gradual to both the north and south.

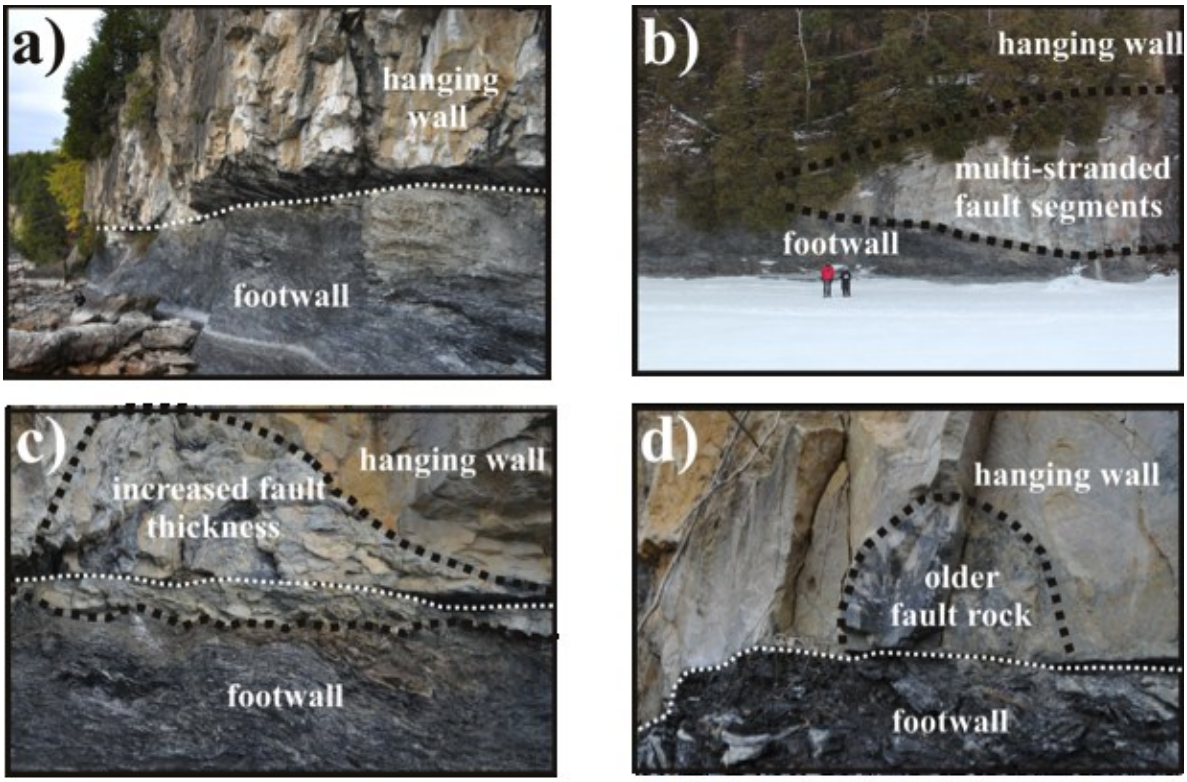

Figure 14. Main structures observed at Champlain Thrust fault: (a) principal slip surface, (b) multi-stranded fault segments (station 2 in Fig. 13a), (c) increased fault thickness (station 6 in Fig. 13d), (d) older abandoned fault rock (station 4 in Fig. 13d). Thin dashed white line follows the principal slip surface, thicker black dashed line follows main structural features.

Given the field observations collected at the Champlain Thrust fault, it is evident that the fault core structure thickness and rock type changes on the scale of a few meters, over an outcrop study length of ~700 m. The preserved fault zone architecture is the cumulative influence of the

entire history of fault motion, as well as the more recent effect of steep normal faults offsetting the original thrust plane. The nearly complete healing of early fault breccias in hanging wall embayments, and elevated concentrations of calcite in the healed breccias, indicates that ancient fluid flow played an important role in re-sealing and healing the fault while it was still active. The crosscutting relationship between the healed breccias and the principle slip surface shows that following healing, the fault slip was more localized onto a discrete slip surface. The variations in fault architecture, such as splaying into multiple strands or broadening of the fault core, may contribute to the present-day permeability structure of this ancient fault. For example, the calcite-cemented volumes of older fault rock are likely significantly more soluble in fresh water than the surrounding dolostone, and so may influence the evolution of karst systems as discussed below.

4.4. Localized groundwater flux from ice seeps

Groundwater seeps are common along cliff-faces of fractured and faulted rock, as fractures provide a pathway for fluid flow out of the subsurface (Chapter 3). The distribution and flux of groundwater seepage is a function of the distribution of permeability (Deitchman and Loheide, 2009,) which in fractured bedrock is controlled by fracture networks. Thus, examining seeps can provide valuable information about the fracture networks and permeability of the rock mass, in addition to providing a minimum elevation of the water table. Detailed observations of frozen seeps an abandoned quarry in a similar climate indicate that the seeps can freeze over in extreme cold events (< -20° C) but generally the groundwater inexorably flows onto the cliff face slowly increasing the volume of the frozen seep when air temperatures are below 0° C (Chapter 3). Therefore the cumulative volume of the frozen seep after a period of freezing temperatures is a time-integrated average of the groundwater flow from that seep.

In February 2014, the Lone Rock Point thrust fault outcrop was surveyed for frozen groundwater seeps from the frozen surface of Lake Champlain. Detailed surveys were made in the footwall throughout the outcrop, but were not possible at the fault and hanging wall in some areas due to difficulty of access. Twenty-three ice seeps were identified, of which nineteen were readily accessible and therefore selected for analysis. In addition to optical photographs, physical observations, such as seep location, notable geologic features, and seep ice deposit height, width, and depth, were recorded. The seep height, width, and depth were used to approximate the volume of groundwater at each seep (Table 3). These volumes were then used to estimate the

flow of each seep, using an estimate of time it took to freeze the seeps, determined from air temperature in the weeks preceding the site visit. As the hanging wall and fault were inaccessible at the southern section of panorama (a), panorama (b), and northern section of panorama (c) (Fig. 13), the seep observations may be biased towards the footwall.

Table 3. Location of ice seep, approximate volume and flow (* = down section of normal fault).

Seep number	Seep location	Seep height above Lake Champlain (m)	Approximate volume (m^3)	Flow (m^3/s)	Sum of seep flows (m^3/s)
1	Hanging wall*	1.83	0.408	2.25E-07	1.75E-5
2	Hanging wall*	1.83	0.202	1.11E-07	
3	Hanging wall*	1.83	0.218	1.20E-07	
4	Fault core	1.07	0.001	7.42E-10	
5	Fault core	1.52	0.013	7.29E-09	
6	Footwall	2.04	14.57	8.03E-06	
7	Footwall	2.04	0.735	4.05E-07	
8	Footwall	2.13	0.006	3.27E-09	
9	Footwall	2.74	0.019	1.07E-08	
10	Footwall	2.44	0.063	3.46E-08	
13	Footwall	1.83	0.153	8.41E-08	
16	Footwall	1.88	0.264	1.46E-07	
17	Footwall	2.25	2.17	1.19E-06	
18	Footwall	2.22	1.79	9.88E-07	
19	Footwall	2.08	0.540	2.98E-07	
20	Footwall	2.08	0.119	6.59E-08	
21	Footwall	2.08	0.052	2.88E-08	
22	Fault core	2.67	10.45	5.76E-06	
23	Fault core	3.43	0.007	3.87E-09	

The majority of the ice seeps (~70%) occurred in the footwall suggesting the heavily fractured and folded footwall has localized permeability pathways. Three seeps occurred in the hanging wall in the section where a later normal fault has down dropped the hanging wall near the lake level (station 1, Fig. 13). Two seeps occurred at the location where the fault core expands into multiple splays (station 2, Fig. 13; Fig. 15a). Two seeps occurred in the fault core (Fig. 15b). The occurrence of seeps at fault intersections like these indicates that the fault in these areas may be acting as conduits, channeling groundwater flow out of the subsurface. No

seeps were found in the older, healed fault breccias, suggesting that there is no significant difference between the healed breccias and the surrounding hanging wall dolostone.

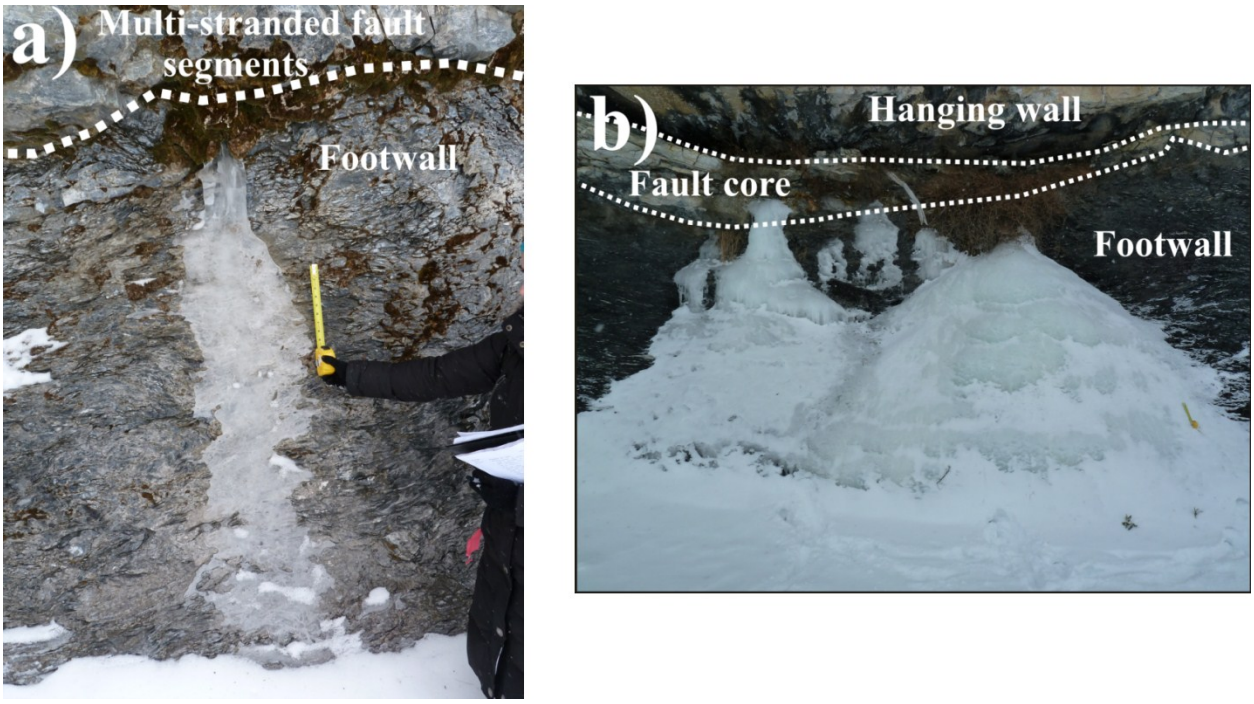

Figure 15. Optical photograph of (a) seep 5 (located at the intersection of the multi-stranded fault segment structure and the footwall), and (b) seep 22 (originating in the fault core). Thin dashed white line follows the principal slip surface. Note measuring tape for scale (1 foot).

On average, ice seeps in the footwall had the largest groundwater flow, which could be due to higher permeability or a higher water table gradient since the footwall is at lower elevations. The seeps in the hanging wall had the second largest flow, followed by the seeps in the fault core. The fault core itself had one large seep that had a large flow (5.76×10^{-6} m/s), but on average, the flows from the fault core were less (in the range of 10^{-9} and 10^{-10} m/s). There is no discernable relationship between seep flow and elevation, suggesting that water table gradient is not the primary control on seep flow.

Groundwater seeps provide a minimum elevation of the water table. The only seeps in the hanging wall (seeps 1-3) were found where the hanging wall is near the lake elevation due to a late normal fault. The lack of seeps in the hanging wall suggests that the water table at the outcrop is approximately at the elevation of the fault.

4.5. Fault geometry and hydrogeology from well data

Drilling and aquifer pumping tests can reveal fault geometry as well as quantify fracture density, hydraulic connections and the hydraulic parameters of an aquifer. Rock core retrieved from boreholes can also useful for determining rock stratigraphy and fracture patterns.

Two 0.15 m wells (CT1 and CT2, Fig. 12) were drilled along strike in November 2013. Rock chips were collected from the wells at 1.5 m intervals to determine the rock lithology with depth. Both wells were drilled through the fault (Fig. 16a). In CT1, rock chips of hanging wall dolostone were recovered from 6.4 – 25.9 m, with the fault at ~27.4 m. A void of 1.83 m was present below the fault, (due to karst), which terminated drilling below this depth due to pressure losses. In CT2, the hanging wall was recorded from 8.2 – 69.8 m below surface. At ~70 m, the footwall is present, and continues to the end of the well (152.4 m).

The large difference in fault depth between the two wells (>30 m) may be due to the normal fault (striking 306° with dips ranging from 50° to 89°) present at station 1 in Fig. 13. Although the projection of the fault from the beach exposure toward the well field is uncertain, it is possible that the fault or a related, similarly oriented fault passes directly between these two well locations.

In March 2014, a third well was drilled using diamond drilling, yielding rock core for lithological and structural analysis. Similar to CT1, karst (2.13 m void) was present in CT3 at ~38.1 m, resulting in the termination of drilling. Due to this, CT3 did not reach the core of the Champlain Thrust fault. The hanging wall rock was composed of fresh grey to buff-colored dolostone with light grey to white crystalline carbonate veins. At 36.6 m, the core degraded into chalky, friable and weathered rock. This, and the increased frequency of fractures at this depth, suggests that the drilling ended at or very near the main fault, and that the rocks were subject to local dissolution by groundwater.

The wells were completed using 0.61 m Polyvinyl Chloride (PVC) piezometers in October 2014 (Fig. 16b). CT1 was screened at the fault (24.4 – 27.4 m) and sealed with sand and bentonite. CT2 was completed with two piezometers; one was screened at the fault (67.1 – 73.2 m), and the other was screened in the footwall (91.4 – 121.9 m). A layer of sand was placed around each screen, and then sealed with a layer of bentonite. CT3 was screened in the hanging wall (32 -38.1 m), and completed with a layer of sand and bentonite around and above the screen, respectively.

We observed strong hydraulic connections during drilling and the installation of piezometers in the wells. During the drilling of CT2, at ~38.1 m, bubbles appeared in the groundwater-filled trench (made by drillers for mud circulation) beside CT1, and the ground surrounding CT1 began to heave and collapse. Additionally, while installing the piezometer in CT3 (at 36.6 m), water overflowed from the piezometers in CT2 (fault) and CT1 (fault). This suggests that as the piezometer advanced to greater depth, groundwater was being displaced through a conduit(s) that connects the wells, leading to flowing artesian conditions in CT2 (fault) and CT1 (fault). These observations, together with the void space noted during drilling (resulting in pressure losses), suggests that there may be a karst network connecting these depths, creating pathways for groundwater to flow out of the nearby piezometers. Karst was not reported in previous studies of the Champlain Thrust fault in Burlington (Stanley 1987; Stanley and Ratcliffe, 1983, 1985; Rowley, 1983), and was not noted in our surface outcrop studies. However, microkarst is present in the Dunham Fm. in the Briton Quadrangle in Connecticut, which is caused by solution enlargement of fractures in fracture zones (J. Kim, Personal Communication, 2014). The role of karst in groundwater flow at the Champlain Thrust fault is difficult to constrain, since the distribution of subsurface karst conduits cannot be mapped from the surface or predicted from structural models.

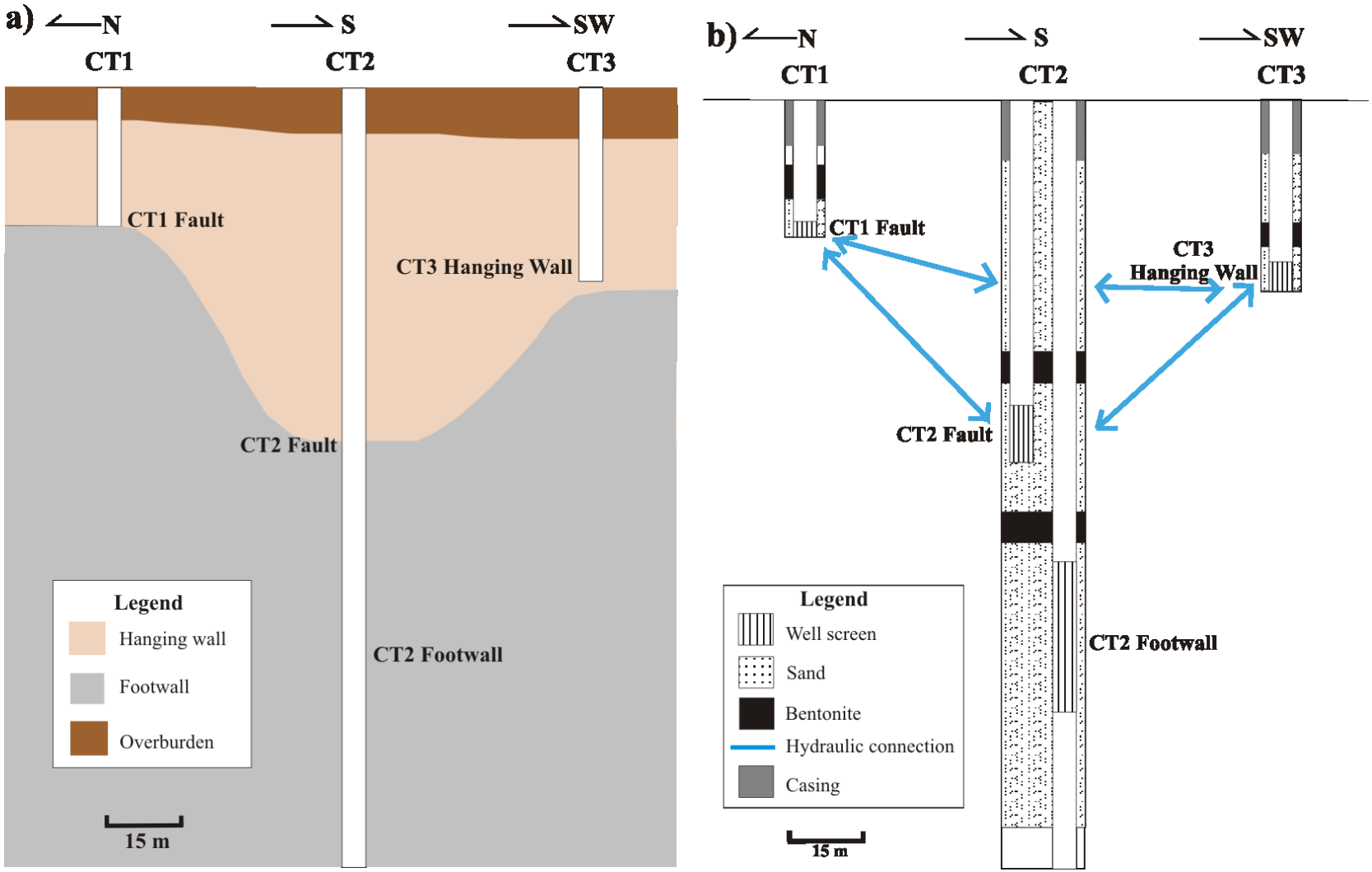

Figure 16. Cross-section of (a) geology; (b) well completion and hydraulic connection observed from well drilling and piezometer installation.

Aquifer pumping tests were completed in CT1 (fault) and CT3 (hanging wall) in May 2015 using a Grundfos Redi-Flo 2 pump. The aquifer pumping test in CT1 (fault) was completed for 12 hours at a pumping rate of 270 mL/sec, while the aquifer pumping test in CT3 (hanging wall) was completed for 9 hours at a rate of 330 mL/sec. The tests in CT2 fault and footwall were unable to be completed due to pump limitations. Solinst level loggers were placed in the non-pumping (observation) wells to record water level changes throughout the aquifer pumping test and manual water level measurements were made in the pumping well during the test. The hydraulic properties of the aquifer were determined using Aqtesolv, an aquifer-testing analysis software (Duffield, 2007). Various analytical models were explored and it became clear that no single model could explain the pumping test responses in these wells given their varied placement with respect to the fault. This suggests that the hydrogeology of the area is complex and that an integrated conceptual model is needed. Therefore, the most appropriate model for each test was used to solve for the aquifer parameters (Table 4 and 5). Analyzing the system using different analytical models is not a common approach, but allows for the different response types to be captured.

Table 4. Hydraulic conductivity and specific storage of each well during the 12-hour CT1 fault pumping test.

Hydraulic Property	CT1 fault (pumping well)	CT2 fault	CT2 footwall	CT3 hanging wall
K (m/s)	1.43E-06	2.05E-06	2.05E-06	4.52E-06
Ss (m^{-1})	-	2.98E-04	2.84E-04	1.94E-06

Table 5. Hydraulic conductivity and specific storage of each well during the 9-hour CT3 hanging wall aquifer pumping test.

Hydraulic Property	CT3 hanging wall (pumping well)	CT1 fault	CT2 fault	**CT2 footwall**
K (m/s)	1.22E-06	4.56E-07	5.65E-08	**1.34E-06***
Ss (m^{-1})	-	1.18E-09	5.46E-07	**1.65E-04***

***Note:** Hydraulic properties of CT2 footwall were solved using the Gringarten and Witherspoon solution for fractured aquifers with a single vertical plane fracture. The other wells were solved using the Hantush (leaky) method.

The best model to explain the response from the CT1 (fault) aquifer-pumping test is the Gringarten-Witherspoon (vertical fracture) model (Table 4; Fig. 17). The derivative (as per Spane Jr. and Wurstner, 1983), and the drawdown curve of the pumping well CT1 fault is linear throughout most of the test, suggesting that a dominant fracture (likely vertical, but possibly horizontal) intersects the pumping well or is situated close by. The pumping test responses at the three observation wells (CT2 fault, CT2 hanging well and CT3 hanging wall) are all appropriately modeled using the Gringarten-Witherspoon method for observation wells that are situated at some distance to the vertical fracture. The hydraulic conductivity calculated from CT3 (using an aquifer thickness of 6.096 m), is characteristic of limestone/dolostone (10^{-6} – 10^{-9} m/s; values obtained in Freeze and Cherry, 1979), while the hydraulic conductivity calculated from CT2 (footwall) is higher than expected for intact shale formations, which is 10^{-9} – 10^{-13} m/s. However, the footwall, (as observed from the outcrop) is heavily fractured and faulted. Unsealed fractures and faults would provide extra pathways for fluid flow, increasing the hydraulic conductivity of the formation. This is most likely the case for CT2 (footwall). The hydraulic conductivity calculated from CT1 (fault) and CT2 (fault) are very similar. The average specific storage value (1.95×10^{-4} m^{-1}) of the aquifer as determined from the results for CT3 (hanging wall), CT2 (fault), and CT2 (footwall) is characteristic of confined aquifers, with higher values obtained for the CT2 (fault and footwall) compared to CT3 (hanging wall). The specific storage of the aquifer as determined from the CT1 (fault) is not representative of the aquifer because the method simply uses the well radius.

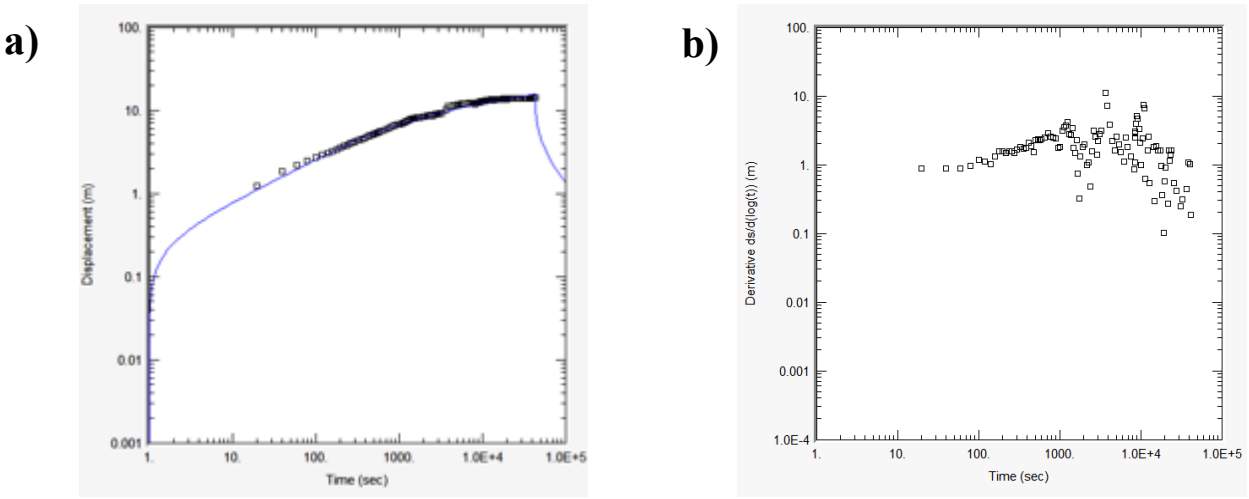

Figure 17. a) Drawdown and b) derivative of CT1 (fault) during the 12-hour aquifer-pumping test.

The best model to explain the responses of the pumping test in CT3 (hanging wall) is the Hantush (leaky) model (Table 5; Figure 18). A radial-type flow regime is established resulting in an almost perfect leaky response in the pumping well itself and the two zones most connected to the CT3 – namely the CT1 (fault) and CT2 (fault). The response at CT2 (footwall) during this test is best explained by the Gringarten-Witherspoon model (as above), which emphasizes that this observation well is influenced by a high permeability connection zone. Similar to the CT1 aquifer pumping test, the hydraulic conductivity calculated from CT3 (hanging wall) during this test is characteristic of limestone/dolostone, but the hydraulic conductivity calculated from CT2 (footwall) is higher than expected for intact shale formations. The hydraulic conductivity values calculated from CT2 (fault) and CT1 (fault) are similar, with CT2 fault being slightly lower than CT1 (fault). The average specific storage value (5.52×10^{-5} m^{-1}) of the aquifer as determined from the results for CT1 (fault), CT2 (fault), and CT2 (footwall) is characteristic of confined aquifers, with higher values obtained for the CT2 (fault and footwall) compared to CT1 (fault). The specific storage of the aquifer as determined from the CT1 (fault) is not representative of the aquifer because the method simply uses the well radius.

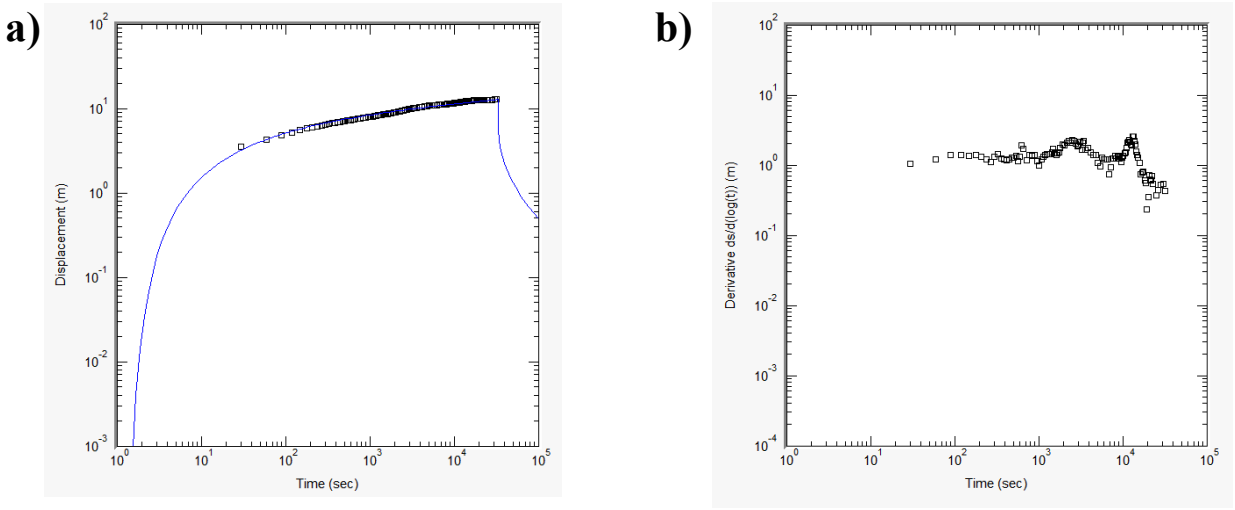

Figure 18. a) Drawdown and b) derivative of CT3 (hanging wall) during the 9-hour aquifer-pumping test.

Even though multiple analytical models were used to interpret the aquifer pumping tests in CT1 (fault) and CT3 (hanging wall), the results are generally consistent between the tests and with the fault geometry and hydraulic connections observed during drilling and well completion. We acknowledge that the parameter estimations are approximate, but our choices of analytical

models are appropriate from a hydrogeological perspective. As such, we accept the uncertainty in our hydraulic parameter estimates, but from these preliminary tests, we can tentatively conclude that the Champlain Thrust is a semi-confined (leaky) aquifer with a strong presence of vertical fractures at the fault, possibly the normal faults exposed in outcrop. The hydraulic conductivities determined from CT2 (footwall) and CT3 (hanging wall) are similar between the tests, even though the hydraulic conductivity from CT2 (footwall) is higher than expected for shale formations. The main difference between the tests is that the hydraulic conductivities calculated from CT1 (fault) and CT2 (fault) determined from the CT3 (hanging wall) pumping test were lower than those determined from the CT1 (fault) pumping test. Additionally, the specific storage values differ for all wells between the tests, but are consistent with values for confined aquifers. However, due to the strong leaky response from the CT3 (hanging wall) aquifer-pumping test, we can infer that the aquifer may be semi-confined.

The results from the aquifer pumping tests are preliminary, and may be biased by a number of factors. Using multiple analytical models to solve for the hydraulic parameters is not standard practice. Each model has its own set of assumptions. The Gringarten-Witherspoon method is appropriate for analyzing pumping test data from a pumping well situated along a vertical fracture and data from observation wells situated at different distances from that fracture. But, if a well off the fracture is pumped, this method is no longer suitable; therefore, an alternative model, here Hantush, is more appropriate. Ideally, pumping test data should be analyzed using a single analytical method that best represents the field site, but in complex hydrogeological settings, we argue that multiple models are best used.

Another limitation is that the length of the two aquifer-pumping tests differed, with the CT1 (fault) test being three hours longer. Hydraulic parameters are better constrained with longer tests, so it is possible that the tests should have been performed for a longer period (24 - 48 hours). Most notably, the results are limited by the small number of wells. Aquifer parameters are best characterized by multiple long-term tests in different locations and within different geologic formations. Therefore, to fully understand the hydrogeology of the Champlain Thrust fault at Lone Rock point, more wells are needed, and aquifer-pumping tests should be performed in *all* structural features (hanging wall, fault and footwall). The presence of karst certainly affected the drilling and pumping tests, terminating drilling in CT1 at the fault and CT3 in the

hanging wall. Future drilling plans in this area must proceed with caution and avoid the karst regions in order to successfully characterize the subsurface hydrogeology.

4.6. Discussion: Integrating surface and subsurface data

Table 6 summarizes the key surface and subsurface observations, and how these relate to observations from other data sources. Structural and hydrogeologic observations of the Champlain Thrust fault reveal a complex system, with unexpected features like karst and normal faults playing a significant role. Structural observations of the outcrop revealed that the fault structure thickness of Champlain Thrust fault varies on the scale of a few meters and splays out into multiple strands. The intersection of these two structures may play a role in the evolution of karst, as the calcite-cemented older fault breccia is likely more soluble than the surrounding dolostone. No karst features were noted in the exposed outcrop, yet the well drilling revealed dominant, karstic flow pathways in the hanging wall and fault. This may indicate that volumetrically minor karst pathways can escape detection in outcrop studies but assert control over groundwater flow patterns. The presence of karst introduces an element of unpredictability at the Champlain Thrust fault, because karst conduits cannot be mapped from the surface or predicted from structural models. Therefore, the role of karst in groundwater flow at the Champlain Thrust fault is difficult to constrain, especially with the limited amount of karst data collected from the wells. A number of questions need answering. Is karst concentrated along younger faults that crosscut the Champlain Thrust fault (i.e. normal faults that intersect with the Champlain Thrust fault at the well-field site) or is it prevalent throughout the subsurface, or is it concentrated along the ancient thrust surface? Does karst play a role in lowering the water table elevation at the outcrop?

Table 6. Summary of key surface and subsurface observations.

Key surface observations	Related subsurface observation
1. Gently-dipping, undulating fault geometry locally crosscut by minor normal faults	Depth to fault surface has tens of 10s m offset in short distance, consistent with offset by normal fault
2. Minor changes in fault core thickness	Difficult to determine variation in fault thickness since only one well drilled through fault
3. Seep distribution indicates groundwater flow paths and the water table in fault or footwall	Large, hanging wall fractures (and karst?) drain the hanging wall near the cliff face locally lowering the water table

Key subsurface observations	Related surface observation
1. Significant vertical offset of the fault between wells	Consistent with minor, exposed normal faults
2. Dominant, karstic flow pathways in the hanging wall and fault	Karst features not obvious in exposed hanging wall nor exposed fault core but elsewhere in Dunham formation
3. Water table near surface	

A normal fault was observed in the northern section of panorama A (station 1, Fig. 13), and could be the cause of the significant fault offset observed between wells CT1 and CT2, and vertical fracture flow observed from the aquifer pumping test. However, the distance from the outcrop to the wells is large enough to introduce significant uncertainty in correlating the outcrop observations to the well observations.

The structural observations of the outcrop assisted in the interpretation of the distribution of groundwater seeps. Seeps were common in the footwall, with a few occurring at fault intersections, such as the normal fault, fault core, or where the fault splays out into multiple strands. The footwall is more fractured compared to the hanging wall, so it is likely that unsealed fractures would provide more pathways for groundwater flow and therefore, more seepage. The occurrence of seeps at fault intersections indicates that these faults may be acting as conduits. Groundwater seeps provide a minimum water table elevation suggesting the water table at the outcrop is at the elevation of the fault and flow in the hanging wall is limited. These observations may be biased, however, due to the inaccessibility of the hanging wall for a large portion of the outcrop. Large hanging wall fractures (and possibly karst) would have to drain the hanging wall near the cliff face to locally lower the water table, but fractures such as these, or karst, were not

observed in outcrop. Future investigation should aim to make detailed seep observations at multiple times throughout the year, in order to gain a greater understanding of the seep distribution and water table elevation at the outcrop.

The aquifer pumping tests in CT1 and CT3 reveal a complex hydrogeologic system with karst and steep fractures (normal fault) as strong hydraulic conduits. Tentatively, the Champlain Thrust fault is a semi-confined (leaky) aquifer, with a presence of vertical fractures at the fault due to a younger fault or set of faults cross-cutting the main fault. However, the results from the aquifer pumping tests are preliminary and limited by the lack of long-term pumping test data in all structural features (footwall, fault, and hanging wall).

The purpose of examining groundwater seeps and performing aquifer-pumping tests is to gain a better understanding of the hydraulic properties of the aquifer. The groundwater seeps provide an estimate of the groundwater flux out of the outcrop itself, as well as an approximate water table elevation. The groundwater flux of the aquifer at the well-field site to the outcrop can be determined using Darcy's Law:

$$Q = -KA\frac{dh}{dl}$$

where q is the groundwater flux (m/s); K is the hydraulic conductivity (m/s); A is the area of the outcrop (700 m length, 30 m height); dh is the change in hydraulic head from the wells to the seeps (m) ; and dl is the distance from the wells to the outcrop (m). An effective hydraulic conductivity was calculated for the well-field site, knowing the hydraulic conductivity (determined from the pumping tests) and thickness of each unit. An estimate of groundwater flow was then derived from the effective hydraulic conductivity, the hydraulic gradient between the wellfield and outcrop, and the area of the outcrop below the water table. The groundwater flow from the well-field site to the outcrop is thus ~3.76×10^{-2} m^3/s whereas the groundwater flow of the outcrop determined from frozen seep observations is 1.75×10^{-5} m^3/s. The flows differ by several orders of magnitude, suggesting that the seep flows are not representative of the full permeability of the area. This is likely due to the lower water table elevation in outcrop and/or groundwater flowing elsewhere. It must be noted that the flow values are estimates; the groundwater flows from the frozen seeps were roughly estimated using an approximate volume and approximate freezing time, which may affect the accuracy of the flow estimates. Moreover, seeps are discrete features and therefore not equivalent to the porous media calculated flows

from the aquifer-pumping tests. Refining these estimates in future studies may produce more accurate groundwater flow estimates, and allow a comparison and cohesion between the two methods (aquifer pumping test flows and seep flow observations).

Despite the surface and subsurface methods revealing different features of the hydrogeology of the Champlain Thrust fault (Table 6), we have developed a preliminary conceptual model of the study area (Fig. 19). At the outcrop, the fault core thickens on the meter scale, splays out into multiple strands and is offset by a normal fault. The abundance of groundwater seeps in the footwall suggests that at the cliff face, the water table lowers to the elevation of the fault, making groundwater flow in the hanging wall limited. At the well-field, the main fault is offset by a fault or set of faults. This, combined with localized occurrence of karst, creates a complex hydrogeologic system. In sum, these methods reveal the complexity and heterogeneity of the hydrogeology of the Champlain Thrust fault. Further research, by both structural and hydrogeolgists, are needed to better constrain and understand this complex system.

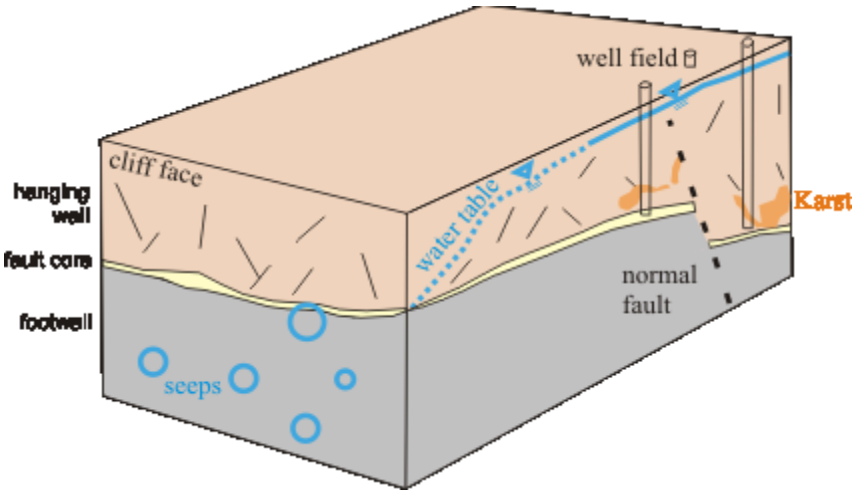

Figure 19. Three- dimensional conceptual model of the Champlain Thrust fault.

4.7. Conclusion

The spectacular exposure of the Champlain Thrust fault at Lone Rock Point is a natural laboratory—where structural and hydrogeological field data can be integrated to understand carbonate thrust fault hydrogeology. In outcrop, the fault core thickness varies on the metre scale, splaying out into multiple strands and is cross-cut by a normal fault. Groundwater seeps are more prevalent in the heavily fractured footwall and limited at fault intersections, such as the normal fault (station 1, Fig. 13), multi-stranded segments of the fault (station 2, Fig. 13), fault core, and the hanging wall. This suggests that at the cliff face the water table in generally located

at the elevation of the fault, and that groundwater flow in the hanging wall is limited. However, these observations are preliminary and may be biased due to the inaccessibly of the hanging wall/fault core.

Results from two aquifer-pumping tests in the hanging wall and fault reveal a complex hydrogeological system. Multiple analytical models were used to estimate the aquifer parameters because the system did not meet any of the strict conceptual model criteria for any particular method. From this, it can tentatively be concluded that the aquifer may be semi-confined (leaky), with a strong presence of vertical fractures at the fault due to a fault or set of faults that cross-cut the main fault at the well-field site. However, these results are preliminary and must be confirmed with long-term tests in multiple wells.

Two striking features were observed from drilling wells near the outcrop – the strong presence of karst and large disparity of fault depth. The normal fault identified along the outcrop, although crudely constrained, may be the cause of this significant offset. These features have a substantial effect on understanding the geology and hydrogeology of the area, and should be further explored in future.

The aim of this paper was to establish an understanding of the hydrogeology of the Champlain Thrust fault using a multi-disciplinary approach. The three approaches (structural geology observations, groundwater seep observations, and hydrogeological observations from wells,) all revealed different aspects of the Champlain Thrust fault, but can be integrated into a preliminary conceptual model (Fig. 19). These methods expose the complexity and heterogeneity of the hydrogeology of the Champlain Thrust fault, an old, well exposed fault in sedimentary rock.

Chapter 5. Summary

This research contributes to a better understanding of fractured carbonate rock hydrogeology. In this study, thermal imagery of groundwater seeps at an unused fractured rock quarry in St. Dominique, Quebec, was collected in order to determine the efficacy of thermal imagery for quantifying groundwater discharge. Additionally, geologic and hydrogeologic observations of the spectacularly exposed Champlain Thrust fault in Burlington, Vermont, were collected to establish a preliminary hydrogeologic understanding of the fault. The results presented in this thesis illustrate the complexity of fractured rock hydrogeology, and the crucial need to for integrated, multi-disciplinary studies to characterize fluid flow in fractured rocks and fault zones.

The first five objectives of this thesis are presented in Chapter 3. The aim was to capture thermal imagery of groundwater seeps at an unused fractured rock quarry in the winter and summer, in addition to capturing a 24-hour time-lapse thermal imagery of two seeps, and create and capture thermal imagery of an artificial seep experiment. Thermal imagery is effective at locating and qualitatively characterizing the flux of groundwater seeps. Areas of active groundwater flow and ice growth can be identified from thermal images in the winter, and low and high flow seeps can be differentiated in the summer. However, the application of thermal imagery is limited by diverse factors including technical issues of image acquisition, diurnal changes in radiation and temperature and rock face heterogeneity. Groundwater discharge rates could not be directly quantified from thermal imagery in either winter or summer because of these limitations. Future research using thermal imagery to characterize groundwater seeps should focus on time-lapse thermal imagery, in order to fully understand the diurnal temperature gradients observed in this study. Time-lapse thermal imagery should be taken in different seasons to see if the diurnal gradients observed in this study are consistent, or how they change throughout the year. This, combined with detailed discharge measurements taken at the seep source, may help determine a quantitative relationship between groundwater discharge and thermal gradients. Although this investigation was conducted at a fractured rock site, our conclusions on the limitations and possibilities of thermal imagery are applicable to other environments where groundwater discharges at discrete locations.

The sixth, seventh, and eighth objectives of this thesis were to determine the prominent structural features of the Champlain Thrust fault, make observations of groundwater seeps present at the outcrop, and determine aquifer parameters from aquifer pumping tests completed in wells drilled near the outcrop (presented in Chapter 4). The main features of the Champlain Thrust fault, as revealed from surface and subsurface data, are different, but were be integrated into a preliminary conceptual model (Fig. 19). In outcrop, the fault core thickness thickens on the meter-scale, splays out into multiple strands and is offset by a minor normal fault. Groundwater seeps are prevalent in the heavily fractured footwall but limited in the fault core and hanging wall, suggesting at the cliff face the water table is generally near the fault core and groundwater flow in the hanging wall is limited. At the well field, low angle fault is offset significantly be a high-angle structure, the water table is near the surface and aquifer pumping tests reveal a complex hydrogeologic system, with karst and steep fractures as strong hydraulic conduits in the hanging wall and fault core. Together the surface and subsurface methods expose the complexity and heterogeneity of the hydrogeology of the Champlain Thrust fault.

Understanding and characterizing the hydrogeology of fault zones is important for numerous environmental concerns. Future research should focus on using integrated, multi-disciplinary methods, which will allow for a more comprehensive understanding of fluid flow in fractured and faulted rocks. The methods used in this thesis (thermal, geologic, and hydrogeologic) reveal the complexities of fractured carbonate rock hydrogeology, but also demonstrate the necessity of integrating these approaches.

References

Agosta, F., and D.L. Kirschner (2003), Fluid conduits in carbonate-hosted seismogenic normal faults of central Italy, *J. Geophys. Res., 108.* http://dx.doi.org/10.1029/2002JB002013.

Agosta, F., Mulch, A., Camberline, P., and A. Aydin (2008), Geochemical traces of CO2 rich fluid flow along normal faults in central Italy, *Geophysical Journal International*, *174,* 758-770. http://dx.doi.org/10.1111/j.1365-46X.2008.03792.x.

Agosta, F., Prasad, M., and A. Aydin (2007), Physical properties of carbonate fault rocks, fucino basin (Central Italy): implications for fault seal in platform carbonates, *Geofluids, 7*, 19-32.

Allen, D., and F.A. Michel (1999), Characterizing a faulted aquifer by field testing and numerical simulation, *Groundwater, 37*(5), 718–728.

Amaefule, J.O., Altunbay, M., Tiab, D., Kersey, D.G., and D.K. Keelan (1993), Enhanced Reservoir Description: Using Core and Log Data to Identify Hydraulic (Flow) Units and Predict Permeability in Uncored Intervals/Wells, Presented at 68th Annual Technical Conference and Exhibition of the Society of Petroleum Engineers.

Anderson, L. J., Osborne, R. H., and D.F. Palmer (1983), Cataclastic rocks of the San Gabriel fault—An expression of deformation at deeper crustal levels in the San Andreas fault zones, *Tectonophysics, 98,* 209–251.

Anderson, M. (2005), Heat as a ground water tracer, *Groundwater*, 43, 951-968.

Andrews, J., Burgess, W., Edmunds, W., Kay, R., and D. Lee (1982), The thermal springs of Bath, *Nature, 298*, 339–343.

Aubry-Wake, C., Baraer, M., McKenzie, J.M., Mark, B.G., Wigmore, O., Hellström, R. Å., and L. Lautz (2015), Measuring glacier surface temperatures with ground-based thermal infrared imaging, Geophys. Res. Lett., 42, doi:10.1002/2015GL065321.

Aydin, A. (2000), Fractures, faults, and hydrocarbon entrapment, migration and flow, *Marine and Petroleum Geology, 17*(7), 797–814.

Baker, H.A., Al-Jawad, S.N., and Z.I. Murtadha (2013), Permeability Prediction in Carbonate Reservoir Rock Using FZI, *Iraqi Journal of Chemical and Petroleum Engineering*, *14(3)*, 49- 54.

Bastesen, E., and A. Braathen (2010), Extensional faults in fine grained carbonates - analysis of fault core lithology and thickness-displacement relationships, Journal of Structural Geology, 32, 1609-1628. doi: 10.1016/j.jsg.2010.09.008

Batelaan, O., and F. De Smedt (2005), Seepage, a new MODFLOW DRAIN Package. *Groundwater*, *42,* 4, 576-588.

Bense, V., Person, M., Chaudhary, K., You, Y., Cremer, N., S. Simon (2008), Thermal anomalies as indicator of preferential flow along faults in an unconsolidated sedimentary aquifer system. *Geophys. Res. Lett.* http://dx.doi.org/10.1029/2008GL036017.

Bense, V.F., Gleeson, T., Loveless, S.E., Bour, O., and J. Scibek (2013), Fault zone hydrogeology, *Earth Science Reviews,* 10.1016/j.earscirev.2013.09.008

Bense, V.F., Van Balen, R.T., and J.J. De Vries (2003), The impact of faults on the hydrogeological conditions in the Roer Valley Rift System: an overview, *Neth. J. Geosci., 82*, 41–53.

Berkowitz, B. (2002), Characterizing flow and transport in fractured geological media: a review. *Adv. Water Resour. 25*, 861–884.

Bethke, C.M., and T.M. Johnson (2008), Groundwater age and groundwater age dating, *Annu. Rev. Earth Planet. Sci., 36*, 121–152.

Billi, A., Valle, A., Brilli, M., Faccenna, C., and R. Funiciello (2007), Fracture-controlled fluid circulation and dissolutional weathering in sinkhole-prone carbonate rocks from central Italy, *J. Struct. Geol., 29,* 385–395.

Boufadel, M., Suidan, M., Venosa, A. and M. Bowers (1999), Steady Seepage in Trenches and Dams: Effect of Capillary Flow, *Journal of Hydraulic Engineering, 125,* 286-294.

Bredehoeft, J.D. (1997), Fault permeability near Yucca Mountain, *Water Resour. Res. 33*(11), 2459–2463.

Breesch, L., Swennen R., and B. Vincent (2009), Fluid flow reconstruction in hanging and footwall carbonates: Compartmentalization by Cenozoic reverse faulting in the Northern Oman Mountains (UAE), *Marine and Petroleum Geology, 26*: 113-128.

Bruhn, R. L., Parry, W. T., Yonkee, W. A., and T. Thompson (1994), Fracturing and hydrothermal alteration in normal fault zones, *Pure and Applied Geophysics, 142,* 609–644.

Brunner, P., Simmons, C.T., and P.G. Cook (2009), Spatial and temporal aspects of the

transitions from connection to disconnection between rivers, lakes and groundwater, *Journal of Hydrology*, *376,* 159-169.

Burbey, T., 2008. The influence of geologic structures on deformation due to ground water withdrawal. Ground Water 46 (2), 202–211. http://dx.doi.org/10.1111/j.1745-6584.2007.00395.x.

Caine, J. S., Coates, D. R., Timoffeef, N. P., and W.D. Davis (1991), Hydrogeology of the Northern Shawangunk Mountains, *New York State Geological Survey Open-File Report*.

Caine, J.S., and S.A. Minor (2009), Structural and geochemical characteristics of faulted sediments and inferences on the role of water in deformation, Rio Grande Rift, New Mexico, *Geological Society of America Bulletin, 121*, 1325-1340.

Caine, J.S., Evans, J.P., and C.B. Forster (1996), Fault zone architecture and permeability structure, *Geology, 24*(11), 1025–1028.

Cardenas, M.B., Harvey, J.W., Packman, A.I., and D.T. Scott (2008), Ground-based thermography of fluvial systems at low and high discharge reveals potential complex thermal heterogeneity driven by flow variation and bioroughness, *Hydrological Processes*, *22,* 980–986.

Celico, F., Petrella, E., and P. Celico (2006), Hydrogeological behaviour of some fault zones in a carbonate aquifer of Southern Italy: an experimentally based model, *Terra Nova, 18*, 308-313.

Chester, F.M., and J.M. Logan (1986), Implications for mechanical properties of brittle faults from observations of the Punchbowl fault zone, California, *Pure Appl. Geophys*., *124*, 80–106.

Deitchman, R. S., and S. P. Loheide II (2009), Ground-based thermal imaging of groundwater flow processes at the seepage face, *Geophys. Res. Lett.*, *36*(14), L14401.

Doan, M.L., and F.H. Cornet (2007), Thermal anomaly near the Aigio fault, Gulf of Corinth, Greece, maybe due to convection below the fault, *Geophys. Res. Lett., 34,* L0631. http://dx.doi.org/10.1029/2006GL028931.

Dorn, C., N.Linde, T.Le Borgne, O.Bour, and M. Klepikova (2012), Inferring transport characteristics in a fractured rock aquifer by combining single-hole ground-penetrating radar reflection monitoring and tracer test data, Water Resour. Res., 48, W11521, doi:10.1029/2011WR011739.

Douglas, M., Clark, I., Raven, K., and D. Bottomley (2000), Groundwater mixing dynamics at a Canadian Shield mine, *J. Hydrol. 235*, 88–103.

Duffield, G.M. (2007), AQTESOLV for Windows Version 4.5 User's Guide, HydroSOLVE, Inc., Reston, VA.

Dugdale, S. J., Bergeron, N. E. and A. St-Hilaire (2015), Spatial distribution of thermal refuges analysed in relation to riverscape hydromorphology using airborne thermal infrared imagery, *Remote Sens. Environ., 160*, 43-55. DOI : 10.1016/j.rse.2014.12.021

Evans, J. P. (1990), Thickness-displacement relationships for fault zones, *Journal of Structural Geology, 12(*8), 1061-1065.

Faulkner, D., Jackson, C., Lunn, R., Schlische, R., Shipton, Z., Wibberley, C., and M. Withjack (2010), A review of recent developments concerning the structure, mechanics and fluid flow properties of fault zones, J. *Struct. Geol. 32*, 1557–1575. http://dx.doi.org/10.1016/j.jsg.2010.06.009.

Flint, A.L., Flint, L.E., Kwicklis, E.M., Bodvarsson, G.S., and J.M. Fabryka-Martin (2001), Hydrology of Yucca Mountain, *Reviews of Geophysics, 39*, 447-470.

Freeze, R.A., and J. A. Cherry (1979), *Groundwater*. Prentice Hall, Inc., Upper Saddle River, New Jersey.

Giurgea, V., Rettenmaier, D., Pizzino, L., Unkel, I., Hotxl, H., Forster, A., and F. Quattrocchi (2004), Preliminary hydrogeological interpretation of the Aigion area from the AIG10 borehole data, Tectonics, 336, 467–475.

Goldscheider, N., and D. Drew (Eds.) (2007), Methods in Karst Hydrogeology. Taylor & Francis, London.

Grandjean, G., and J.C. Gourry (1996), GPR data processing for 3D fracture mapping in a marble quarry (Thassos, Greece), *Journal of Applied Geophysics, 36*, 19-30.

Hare, D.K., Briggs, M.A., Rosenberry, D.O., Boutt, D.F., and J.W. Lane (2015), A comparison of thermal infrared to fiber-optic distributed temperature sensing for evaluation of groundwater discharge to surface water, *Journal of Hydrology, 530,* 153-166. ISSN 0022-1694, http://dx.doi.org/10.1016/j.jhydrol.2015.09.059.

Hayman, N. W., and W.S.F. Kidd (2002), Reactivation of prethrusting, synconvergence normal faults as ramps within the Ordovician Champlain-Taconic thrust system, *Geological Society of America Bulletin, 114,* 476-489.

Jourde, H., Flodin, E.A., Aydin, A., Durlofsky, L.J. and X.H. Wen (2002), Computing permeability of fault zones in eolian sandstone from outcrop measurements, *Am. Assoc. Pet. Hydro.*, *Bull 86*, 1187-1200.

Kim, J. (2014), Personal communication.

Kim, J., Ryan, P., Klepeis, K., Gleeson, T., North, K., Bean, J., Davis, L., and J. Filoon (2014), Tectonic evolution of a Paleozoic thrust fault influences the hydrogeology of a fractured rock aquifer, northeastern Appalachian foreland, *Geofluids, 14*(3)*,* 266-290.

Kolyukhin, D., and A. Torabi (2012), Statistical analysis of the relationships between faults attributes, *J. Geophys. Res., 117*, B05406, doi:10.1029/2011JB008880.

Kulander, B.R., Dean, L.S., and B.J. Ward (1990), Fractured Core Analysis: Interpretation, Logging and Use of Natural and Induced Fractures in Core, *AAPG Methods in Exploration Series. No. 8,* American Association of Petroleum Geologists, Tulsa, OK.

Lemieux, J.M., Therrien, R., and D. Kirkwood (2006), Small scale study of groundwater flow in a fractured carbonate-rock aquifer at the St. Eustache quarry, Quebec, Canada, *Hydrogeology Journal, 14* (4), 603-612.

Liu, W-Y, Gantt, R.T., and A. Klemas (1987), Measurement of the surface emissivity of turbid waters, *Remote Sensing of Environment, 21*, 97 – 109.

Loheide, S. P., and S. M. Gorelick (2006), Quantifying stream − aquifer interactions through the analysis of remotely sensed thermographic profiles and in situ temperature histories, *Environ. Sci. Technol.*, *40* (10), 3336–3341.

Long, J. C. S., and D.M. Billaux (1987), From Field Data to Fracture Network Modeling:

Lopez, D. and L. Smith (1996), Fluid flow in fault zones: Influence of hydraulic anisotropy and heterogeneity on the fluid flow and heat transfer regime, *Water Resour. Res., 32*(10), 3227-3235.

Lunn, R.J., Shipton, Z.K., and A.M. Bright (2008), How can we improve estimates of bulk fault zone hydraulic properties? In: Wibberley, C., Kurz, W., Imber, J., Holdsworth, R., Collettini, C. (Eds.), The Internal Structure of Fault Zones: Implications for Mechanical and Fluid-flow Properties. Vol. 299 of Special Publications. Geological Society, London, 231–237. http://dx.doi.org/10.1144/SP299.14.

Masuda K, Takashima T, and Y. Takayama (1988), Emissivity of pure and sea waters for the model sea surface in the infrared window regions, *Remote Sensing of Environment, 24*,

313–329.

Mayer, A., May, W., Lukkarila, C., and J. Diehl (2007), Estimation of fault-zone conductance by calibration of a regional groundwater flow model: Desert Hot Springs, California. *Hydrogeol. J.*, *15*, 10931106.

Micarelli, L., Benedicto, A., & Wibberley, C. A. J. (2006). Structural evolution and permeability of normal fault zones in highly porous carbonate rocks, *Journal of Structural Geology*, *28*(7), 1214-1227.

Mozley, P.S., and L.B. Goodwin (1995), Patterns of cementation along a Cenozoic normal fault: A record of paleoflow orientations, *Geology, 23*, 539-542.

Novakowski, K.S., Sudicky, E.A., and P. Lapcevic (2007), Groundwater flow and solute transport in fractured media, In: *Groundwater Engineering*, 2nd Edition, Ed: J. Delleur, CRC Press.

Pandey, P., T. Gleeson, and M. Baraer (2013), Toward quantifying discrete groundwater discharge from frozen seepage faces using thermal infrared images, Geophys. Res. Lett., 40, 123–127, doi:10.1029/2012GL054315

Pfister, L., McGonnell, J.J., Hissler, C., and L. Hoffman (2010), Ground based thermal imagery as a simple practical tool for mapping saturated area connectivity and dynamics, *Hydrological Processes, 24,* 2123-2132.

Ratcliffe, N.M., Stanley, R.S., Gale, M.H., Thompson, P.J., and G.J. Walsh (2011), Bedrock geologic map of Vermont, U.S. Geological Survey Scientific Investigations Map 3184, 3 sheets, scale 1:100,000.

Romanoa, C. G., Frind, E.O., and D.L. Rudolph (1999), Significance of unsaturated flow and seepage faces in the simulation of steady-state subsurface flow, *Groundwater, 37*, 625–632, doi:10.1111/j.1745-6584. 1999.tb01151.x.

Rowley, D. B., and W.S.F. Kidd (1981), Stratigraphic relationships and detrital composition of the medial Ordovician flysch of western New England: Implications for the tectonic evolution of the Taconic orogeny, *The Journal of Geology*, 199-218.

Rowley, D.B. (1983), Contrasting fold-thrust relationships along northern and western edges of the Taconic allochthons; Implications for a two-stage emplacement history, *Geological Society of America Abstracts with Programs, 15*, 174.

Rugh, D. and T. Burbey (2008), Using saline tracers to evaluate preferential recharge in fractured

rocks, Floyd County, Virginia, USA, *Hydrogeology Journal, 16,* 251-262.

Scholz, C., and C. Anders (1994), The permeability of faults*, Proceedings of Workshop LXIII, The Mechanical Involvement of Fluids in Faulting, U.S. Geol. Surv. Open File Rep.* 94-*228*, 247-253.

Schuetz, T. and M. Weiler (2011), Quantification of localized groundwater inflow into streams using ground-based infrared thermography. *Geophysical Research Letters*, *38*: L03401.

Séjourné,, S. and M. Malo (2007), Pre-, syn-, and post-imbrication deformation of carbonate slices along the southern Quebec Appalachian front – implications for hydrocarbon exploration, *Canadian Journal of Earth Sciences*, *44*(4), 543-564, 10.1139/e06-106

Shea, C., Jamieson, B. and K.W. Birkeland (2012), Use of a thermal imager for snow pit temperatures, *The Cryosphere, 6,* 287-299.

Shipton, Z., Evans, J., Kirchner, D., Kolesar, P., Williams, A., and J. Heath (2004), Analysis of CO_2 leakage through low-permeability faults from natural reservoirs in the Colorado Plateau, southern Utah, In*: Baines, S., Worden, R. (Eds.), Geological Storage of Carbon Dioxide. Vol. 233 of Special Publications*. Geological Society, London, 43–58.

Sibson, R. H. (1977), Fault rocks and fault mechanisms, *Geological Society of London Journal*, *133*, 191–231.

Simpson, M. J., Clement, T. P., and T.A. Gallop (2003), Laboratory and numerical investigation of flow and transport near a seepage-face boundary, *Groundwater*, *41*, 690 – 700, doi:10.1111/j.1745-6584.2003.tb02407.x.

Smith, L., Forster, C. B., and J.P. Evans (1990), Interaction between fault zones, fluid flow and heat transfer at the basin scale, in: *Hydrogeology of low Permeability environments,* (S. P. Newman and I. Neretnieks, eds.), International Association of Hydrological Sciences selected papers in Hydrogeology, 2, 41-67.

Sorkhabi, R., and Y. Tsuji (2005), Faults, Fluid Flow& Petroleum Traps, *AAPG Memoir, vol. 85*, American Association of Petroleum Geologists.

Spane, F. A. and S.K. Wurstner (1993), DERIV: A Computer Program for Calculating Pressure Derivatives for Use in Hydraulic Test Analysis, *Groundwater, 31*, 814–822. doi: 10.1111/j.1745-6584.1993.tb00855.x

Stanley, R. (1987), The Champlain Thrust Fault, Lone Rock Point, Burlington, Vermont, *Geological Society of America Centennial Field Guide—Northeastern Section.*

Stanley, R. S., and N.M. Ratcliffe (1983), Simplified lithotectonic synthesis of the pre-Silurian eugeoclinal rocks of western New England, *Vermont Geological Survey Special Bulletin No. 5*.

Stanley, R. S., and N.M. Ratcliffe (1985), Tectonic synthesis of the Taconic orogeny in western New England, *Geological Society of America Bulletin, 96*, 1227-1250.

Vollmer, M., and K.-P. Möllmann (2010), Fundamentals of infrared thermal imaging, *Infrared Thermal Imaging*, 1–72, Wiley-VCH Verlag GmbH & Co. KGaA, Weinheim, Germany.

Waldick, M. K., and B. Conant (2006), Evaluation of land-based infrared thermography to identify and quantify groundwater discharge to a small stream, *Paper 13-8, Geological Society of America Annual Meeting and Exposition,* 22–25 October, Philadelphia, Pennsylvania.

West, A.C.F., Novakowski, K.S., and S. Gazor (2005), Usefulness of core logging for the identification of conductive fractures in bedrock, *Water Resour. Res., 41,* W03018, doi:10.1029/2004WR003582.